Summer 7-1-2022

Effects of Surface Topography on Macrophages and Bacterial Cells

Joseph Carnicelli
Syracuse University

Abstract:

An association has been found between the texture of breast implants and anaplastic large cell lymphoma, which led to some textured implants to be withdrawn from the market in 2019. There is evidence that these cancers are associated with the harboring of bacteria on the surfaces of the textured implants. It is possible that specific topographic features hinder the removal of attached bacteria by inhibiting macrophage phagocytosis or promoting biofilm formation. Here we examine how bacteria and macrophages interact with recessive surface topographies as analogs to the surfaces seen on textured breast implants. Changes in bacteria morphology were observed among the cells attached in deep recessive features. There was a preference for macrophage overlap with surface topography, particularly for recesses around 5x5 μm in size. These results indicate that certain topography could affect localization of bacteria and macrophages to the recesses of the surface, while other topographies could enhance biofilm formation and filamentation of bacteria in recesses and thus hinder phagocytosis. Quantification of phagocytosis on different topographies showed a decrease in bacteria per macrophage on 5 μm wells compared to flat surfaces. It was also seen that deeper 30 μm topography had less phagocytosis compared to shallower 10 μm deep patterns, and macrophages inside of 30 μm deep wells phagocytosed less bacteria than those outside of the wells. In summary, the findings of this study suggest that certain topographic features can reduce phagocytosis of bacteria and thus contribute to long-term biofilm formation and complications.

Effects of Surface Topography on Macrophages and Bacterial Cells

By

Joe Carnicelli

B.E., SUNY Binghamton, 2017

M.S., Cornell University, 2018

Thesis

Submitted in partial fulfillment of the requirements for the degree of

Master of Science in Bioengineering

Syracuse University

July 2022

Acknowledgements

I would like to thank Dr. Ren for his support and guidance in my research. I would like to thank Dr. Gu for her mentorship through my studies. I would also like to thank the NSF for providing funding for my work.

Table of Contents

List of Figures

1. Introduction

Biofilms

Antibiotic resistance infections are a persistent problem for the application of medical devices. According to the CDC, there are over 2.8 million antibiotic resistant infections in the United States per year, with more than 35,000 deaths[1]. When bacteria settle on a surface, the attached cells secrete an external, protective matrix, forming a biofilm. Biofilms confer antibiotic resistance to bacteria and protect individual cells from phagocytosis by a host immune system[2]. The development of biofilm on an implanted medical device thus leads to chronic infections that are difficult to treat. In fact, up to 80% of all chronic infections in humans are associated with biofilms[3]. There is potential to improve chronic infections rates by designing medical devices. These challenges motivate research on antifouling technologies to minimize the colonization of bacteria and biofilm growth.

BIA-ALCL

Infections, including viruses, can also play a role in the development of cancer, accounting for about 20% of all cases worldwide[4]. Cancer formation is often the result of sustained inflammation[4]. Because of this, chronic microbial presence may trigger cancer development. There is considerable evidence for this in the case of *H. pylori* infections and gastric cancer[5,6]. Chronic stimulation with *H. pylori* antigens is also attributed to MALT lymphoma of B cells[7]. Similarly, chronic infection by *C. psittaci* has been linked to ocular adnexal lymphoma[8]. Even commensal bacteria have been seen to play a role in the progression of cancers. One example is T cell lymphoma, which may be promoted by *S. aureus* and other bacteria present on the skin[9].

Disruption of normal microbiota can also lead to cancer, as seen with intestinal dysbiosis and its association with colorectal[4,10].

Recently, the FDA recalled Allergan's textured BIOCELL breast implants due to an association with anaplastic large cell lymphoma (ALCL)[11]. Breast implant-associated ALCL (BIA-ALCL) is a T-cell derived cancer that is similar to primary cutaneous ALCLs. It is believed that these types of cancers derive from chronic inflammation from the prolonged presence of antigens, whether from foreign object particles or microbial antigens.[12] One group saw evidence suggesting that BIA-ALCL is related to the presence of bacteria on the surface textured of the implants[13]. The textured patterns were seen to promote bacterial adhesion compared to smooth surfaces and increased T-cell presence at the implant site.

It has been put forward that there may be a connection between organs that are susceptible to inflammation driven cancer and typical microbial interactions, such as in the lungs and gastrointestinal tract versus inflamed joints[4]. However, in the case of BIA-ALCL, the internal breast tissue and surface of an implant are not normal areas for microbiota to be present. Theoretically, the immune system could eradicate bacterial presence under these conditions. However, in the case of textured implants with higher surface area, such as Allergan BIOCELL, bacteria accumulate more[14] and BIOCELL implants have been linked to the occurrence of cancer on average of 7-10 years after implantation[15]. This leads to the speculation that chronic inflammation from bacterial presence on these implants is the cause for eventual cancer development.

Textured patterns on breast implants add functionality by helping to improve tissue integration with the host so the implants do not dislocate[15]. Since not all textured breast implants have not been linked to BIA-ALCL development, it would suggest that certain topographic parameters

play a specific role in bacteria accumulation and persistence of inflammation, which could eventually lead to ALCL. By furthering the understanding of how bacteria survive on surfaces with different topographies and avoid clearance by the immune system, better implant surfaces could be designed to minimize biofilm accumulation while maintaining the functionality of the surface. This requires not only an understanding of how biofilm formation is affected by surface topography, but also how phagocytes, like macrophages, are affected by the local environment and how these cells interact with bacteria to clear infections.

Macrophage Topography Interactions

To date, little work has been published regarding phagocytosis on different surface topographies. One group used a shape memory polymer to wrinkle SiO_2 films that were deposited on the surface of the polymer, creating a wrinkle pattern with roughness peak-valley measures of 2 μm and 9 μm. They found that phagocytosis of heat-killed *S. pneumoniae* by bone marrow-derived macrophages increased on wrinkled surfaces compared to flat surfaces, with an increased effect for the larger, 9 μm scale, topography.[16] Another study looked at the phagocytosis of polystyrene beads by P388D1 macrophage cell line on nano-grooved topography. The authors reported an increase in the number of macrophages with more than two beads phagocytosed with topography, compared to a flat surface. They also reported an increase in macrophages with more than two beads phagocytosed for 282 nm deep topography compared to 71 nm deep topography[17]. While these studies suggest improved phagocytosis from certain topography, the scales of topographic features shared are still limited and more research is needed to understand how surface properties affect biofilm formation related to BIA-ALCL.

While there is a lack of studies focused on the effects of surface topography and phagocytosis, there are plenty of studies regarding the effects of topography on the phenotype and morphology of macrophages. Nanotopographies appear to promote an M2 anti-inflammatory phenotype. Surfaces coated with gold nanoparticles on the scale of 10s of nanometers were found to decrease the production of inflammatory cytokines, IL-6, IL-1β, and TNF-α, by bone marrow-derived macrophages[18]. Another study looked at RAW264.7 macrophage cell line on hydroxyapatite surfaces with grain sizes varying between 100 nm and 450 nm. The results showed that the smallest grain size led to downregulated M1 markers, such as iNOS and TNF-α, after 5 days of culture. Flowcytometry results showed that the M2/M1 ratio of macrophages on these surfaces increased with decreasing grain size[19]. When Raw 264.7 macrophages were cultured on nanopillars of 300 nm diameter, they adopted a well-spread morphology, whereas 150 nm deep nanopits lead to an elongated morphology. Both nanopillars and nanopits led to an increase in M2, anti-inflammatory, markers[20].

In contrast to nanotopography, macrophage interactions with microtopographies exhibited an increased in pro-inflammatory response. Vassey et al.[21] screened over 2000 pillar patterns (10 μm in height) to understand key geometric features of surface topography that effect macrophages. The study found that macrophage attachment increased with pillar geometries of 5-10 μm, with 5 μm wide pillars having the strongest effect. Macrophages appeared to engulf micropillars on these surfaces, whereas for larger topography, macrophages were in between the pillars. Adsorption of fibronectin and collagen onto their surfaces did not affect the results, leading the group to conclude that the effect of topographic on attachment is stronger than the presence of ECM proteins. Further analysis of cell surface markers showed a trend of increased

M2 phenotype on smaller and more denser pillars, and increased M1 phenotype on larger and more dispersed pillars.

Macrophages have also been seen to align and elongate along parallel grating of 250 nm – 2 μm width[22]. Proinflammatory cytokines were seen to increase in the first 24 hours, with a decrease in the anti-inflammatory cytokine VEGF, but this effect reversed at 48 hours. This suggests that macrophages have an initial inflammatory response to these topographies, but eventually become more anti-inflammatory. Interestingly, this study did not see much of a VEGF increase between 24 and 48 hours of incubation on 1 μm grating, suggesting that this transition to M2 may not be as strong or present on larger, micrometer-scale topographies. One study looked at micro-scale pillars and lined geometry effects on macrophages[23]. Cell markers showed an increased number of proinflammatory cells on pillars 3 um tall/wide with 6 – 23 μm spacing, whereas 20 μm tall/wide pillars with 70 μm spacing showed more anti-inflammatory markers. The cells on the larger pillars were seen to spread in between the large spacing, which may minimize interaction with the topography compared to the smaller spaced pillars, which were seen to sit on top of the pillars. This synergizes with the increase proinflammatory markers seen on the lined geometry which had a close spacing of 20 μm. This provides evidence that interaction with micro-scale topography could promote a pro-inflammatory response in macrophages. Another study looked at microtexture versus nanotexture on PVDF surfaces and saw little effect of the nanotexture on cytokine secretions/gene expression compared to a control surface, whereas the microtextured surface with 1 μm height gave mixed results for M1 and M2 cytokines and gene expression changes from the control[24]. There appeared to be a general trend toward a pro-inflammatory state from microtextured surfaces, but compared to LPS stimulated cells, there are some differences in

M2 indicators, This suggests that the topography could promote an activated phenotype in macrophages that does not cleanly fit into the M1/M2 model.

Bacteria Topography Interactions

A lot of work has been done on controlling biofilms and studying bacteria on different topographies. Nature provides sources of inspiration for this approach with nano-scale architecture acting to avoid bacterial build up on the wings of cicadas[25] and gecko skin[26]. These nanotopographies have been found to kill bacteria. Wang and colleagues[27] were able to kill 99% of *P. aeruginosa* by cycling solution through a flow cell with black silicon nanopillar topography. Another group found over 80% killing after 3 hours for *E. coli* and *S. aureus* on 4 μm tall and 220 nm wide pillars on a silicon wafer[28]. Microbial killing by nano-pillars is believed to result from over-stretching of cell membrane regions in between sharp features on the surface that lead to high enough tension to tear the membrane[29].

Micro-scale topography can also influence biofilm formation and bacterial behavior. One of the best-known examples is the development of Sharklet surfaces based on the microtopography of shark skin. PDMS with Sharklet patterned microtopography, 2 μm width and spacing and 3 μm height, were shown to decrease *S. aureus* biofilm growth of the course of 21 days compared to smooth surfaces[30]. The Ren lab[31] has seen that *E. coli* prefers to form biofilms in the valleys between micropillar topography, yielding more surface coverage (26.9% for 5 μm spacing) than a smooth surfaces (11.6%) after 24 hours. However, *E. coli* growth on top of the pillars was limited for sizes below 20 μm x 20 μm, suggesting a spatial requirement for biofilm development. Similar results were seen in another study looking at micropillars, micropits, and ridges on PDMS surfaces with depths of 115 nm and 20 nm, which saw a general decrease in

bacterial adhesion of 30-45% for *E. coli, S. epidermis*, and *B. subtilis* across all topographies.[32] The study found that there was a preference for bacteria attachment in the recesses of the patterns. Overall, data from the literature suggests that bacterial attachment and subsequent biofilm growth can be promoted or discouraged based on the topography of the surface. This provides an opportunity for the design of surface topographies that minimize bacteria colonization.

More recently it has been seen that dynamic surfaces have the potential to further inhibit biofilm formation and remove established biofilms. Dynamic topographies apply a changing surface structure to mechanically repel/remove bacteria from the surface. Shape memory polymers are a type of polymer that can be fixed in a chosen shape when cooled below their glass transition temperature and return to original form after heating. Typically, these polymers require refixing after each actuation, limiting its potential for medical applications, but recently a reversible polymer that can be actuated through multiple temperature cycles was tested for removing biofilm. The study[33], found that 3 cycles of actuation could remove up to 94.3% of 48-hour biofilm of *P. aeruginosa*. Magnetically actuated surface topography has also been seen to have potential for removing biofilms from surfaces[34]. PDMS micropillars with magnetic nanoparticles in the tips of the pillars were subjected to an external magnetic field to cause a bending motion in the pillars. It was seen that 48-hour *E. coli* biofilms could be removed by 99.7% after 3 min of actuation of magnetic micropillars. By continuously actuating the topography thorough formation of the 48-hour biofilm culture, biomass was 99.8% lower than a static control surface.

Overall, evidence that prolonged inflammation from increased bacteria presence on certain breast implant topography suggests that geometric features of these surfaces create a condition where bacteria can avoid clearance by the immune system. If this is the case, it is important to discern

the different topographic features that could limit elimination of bacteria by phagocytes. This could relate to topographies that favor biofilm growth or that alter leukocyte behavior. In this study, we focus on macrophage interactions with recessive surface patterns as a model system to mimic the recessive topographies seen on textured breast implants. We also examine macrophage and *E. coli* in coculture on these surfaces to determine if certain topographies could interfere with phagocytosis.

2. Materials and Methods

2.1 Media Supplies: DMEM (Thermofisher Cat: 11995-065) with 1% Pen/Strep solution (Thermofisher Cat: 15140-122), DMEM (Thermofisher Cat: 31053-028) containing added sodium pyruvate (1 mM) (Thermofisher Cat: 11360-70) and L-glutamine (4 mM) (Thermofisher Cat: 25030-081). DMEM medias were used with 10% FBS (Thermofisher Cat: 16140-071). LB media was used with bacteria cultures containing either 30 μg/mL tetracycline or 100 μg/mL ampicillin and 2 mg/mL arabinose.

2.2 Cell Culture: RAW264.7 mouse macrophage cell line cultures were maintained in DMEM in tissue culture petri dishes before experiments. E. *coli* RP437/pRSH103 was cultured with 30 μg/mL tetracycline and E. *coli* RP437/pGLO cultured with 100 μg/mL ampicillin and 2 mg/mL arabinose in LB media for about 15 hr before experiments.

2.3 Surface Preparation and Coating: PDMS was mixed at a 10:1 mixing ratio and cured in an oven at either 60 degrees Celsius for 24 hours or 100 degrees Celsius for 1 hour. To create the well topography, PDMS was poured onto a silicon wafer that contained the micropillars that reverse patterns of the desired micro-wells. Well sizes used varied from 2-300 μm in side length and from 2-300 μm in spacing. One wafer produced wells with a 10 μm depth and a second

wafer was used to produce topography with a 30 μm depth. After curing, PDMS samples were sterilized under UV light for a total of 30 min. Samples were then coated with fibronectin (5 μg/mL) in PBS under desiccation for 30 min. The desiccation was used to remove air bubbles from the wells, as done in previous work[35]. After desiccation, large bubbles were removed from the PDMS with a pipette and the samples were allowed to sit for another 5 min. The PDMS samples were then washed 3 times in PBS and dried in the biosafety hood for about 45 minutes. Fibronectin coated samples were stored in the refrigerator until use.

2.4 Macrophage Position Experiments: Fibronectin-coated PDMS samples were desiccated in DMEM for 30 min to remove air bubbles from the wells. Macrophages were then inoculated at 10^5 cells/cm^2 and samples were cultured at 37 degrees Celsius and 5% CO_2. After culture for 3 or 6 hours, samples were imaged on an Axio Observer Z1 fluorescence microscope (Carl Zeiss Inc., Berlin, Germany). Macrophages were counted and categorized based on their positions relative to the topography.

2.5 Coculture Positioning Experiments: Fibronectin-coated PDMS samples were desiccated in LB for 30 min to remove air bubbles from the wells. E. *coli* RP437/pRSH103 was inoculated at OD600 of 0.005 and cultured at 37 degrees Celsius for 2 hours to attach and grow bacteria on the PDMS surfaces. Samples were then washed 3 times in PBS and submerged in a new dish with DMEM (no Pen/Strep and phenol red). Macrophages were then inoculated at 10^5 cells/cm^2 and samples were placed in the mammalian incubator for 3 or 6 hours for coculturing. Samples were then imaged on an Axio Observer Z1 fluorescence microscope (Carl Zeiss Inc., Berlin, Germany) to examine macrophage position. Macrophages were counted and categorized based on their positions relative to the topography. For experiments where bacteria were categorized as “only in the wells”, biofilm were washed in PBS by flipping upside down and rubbing the

surface of the topography in circles a few times. This removed most of the bacteria in between the topography while still preserving some of the bacteria in the wells of the topography.

2.6 Macrophage Tracking Experiments: PDMS samples were desiccated in DMEM for 30 min to remove bubbles from recessive patterns. Raw264.7 macrophages were then inoculated at $2.5*10^4$ or 10^5 cells/cm^2. Cells were imaged through timelapses with an Axio Observer Z1 fluorescence microscope (Carl Zeiss Inc., Berlin, Germany) with a cell chamber heated to ~37 degrees Celsius. ACTIVE and Fiji ImageJ Manual Tracking were used to create tracks for the macrophage movement.

2.7 Macrophage Phagocytosis: Fibronectin-coated PDMS samples were dessicated in LB for 30 min to remove air bubbles from the recessive patterns. E. *coli* RP437/pGLO was inoculated at OD600 of 0.1 with ampicillin (50 μg/mL) and arabinose (2 mg/mL) and cultured for 1 hour to allow an early biofilm form on the surface. Samples were then washed 3 times in PBS and submerged in DMEM (no Pen/Strep and phenol red) and added ampicillin (50 μg/mL) and arabinose (2 mg/mL). RAW264.7 macrophages were then inoculated at 10^5 cells/cm^2 and samples were incubated for 3 hours to allow for phagocytosis. Macrophages were then washed 3 times in PBS, fixed with 3.4% formaldehyde for 15 min, lysed with 0.1% Triton-X 100 for 5 min, and stained with Alexa Fluor 546 phalloidin (Thermofisher Cat: A22283) for 15 min. Samples were then imaged on a microscope slide with an Axio Imager M1 fluorescence microscope (Carl Zeiss Inc., Berlin, Germany). Z-stacks were taken and deconvoluted. Phagocytosis was determined by counting the bacteria inside of macrophages. For some experiments, macrophages were stained with propidium iodide stain instead of phalloidin actin stain.

2.8 Flow Cytometry: Macrophages phagocytosis was measured by flow cytometry following the same procedure mentioned above. After coculture the cells for 3 hours for phagocytosis, cells were removed from the PDMS surfaces with 2 min of sonication and 30 seconds vortexing a setting of 10. Multiple biological replicates were combined to achieve a high enough cell concentration and samples were run on a flow cytometer using GFP and particle size to distinguish macrophages that had fluorescent bacteria in them. Samples were imaged on an Axio Observer Z1 fluorescence microscope (Carl Zeiss Inc., Berlin, Germany) before and after sonication/vortexing for reference.

2.9 Statistics: Statistical comparisons were performed on SAS software using One-way or Two-way ANOVA analysis, check with a tukey test. For Figure 3, a student's t-test was used.

3. Results

3.1 Macrophage Position

Macrophages were cultured on various recessive patterns for 6 hours in DMEM media. By imaging on an inverted microscope, it was seen that the macrophages tend to localize on the recesses on the surfaces. This was initially noted for wells with a 2, 5, and 10 μm side length and 10 μm spacing, as seen in Figure 1, where it is seen that more than 70% of the macrophages are interacting with well topography for each well size. The stacked bar graph in Figure 2 shows that, for 5x5 μm wells, more than 50% of the cells are overlapping at least half of a well, while for 10x10 μm wells the number is around 35%. These data suggest that macrophages have a preference for interacting with well topography.

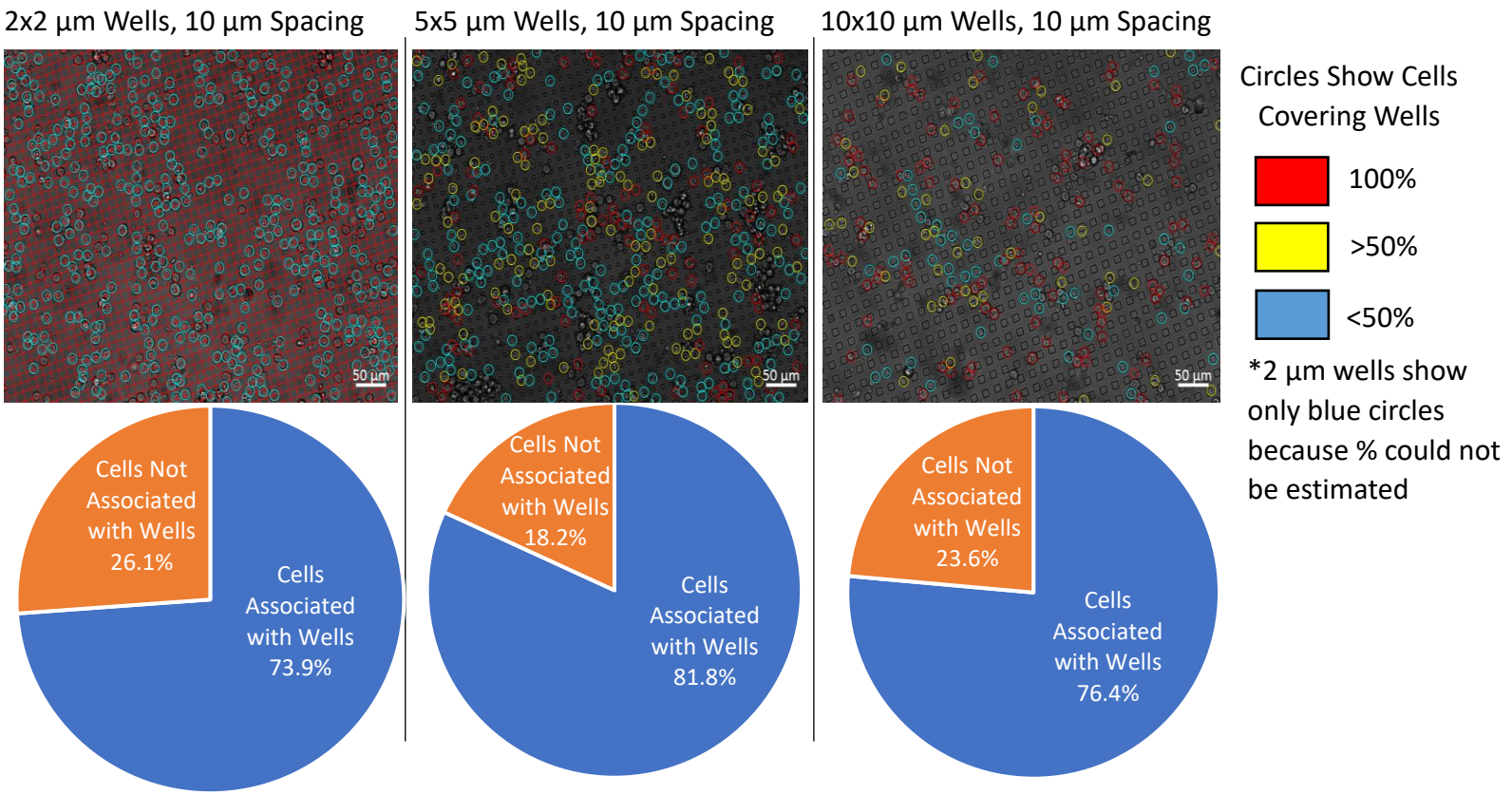

Figure 1: Macrophages on 2x2 µm (left image), 5x5 µm (middle image), and 10x10 µm (right image) circle in colors based on their how much they are overlapping recessive wells on the surface. The pie charts show all the cells touching the well topography (blue) versus those not touching the well topography (orange).

Next, macrophages were examined more quantitatively by counting cells on different topographies and categorizing them based on their locations. It was seen that macrophages have a general preference for interacting with well topographies. This can be seen in Figure 3, which shows the number of macrophages not interacting with well topographies to be lower than expected for a random distribution of macrophages. This is demonstrated in the graph because, for a random distribution of cells, we would expect the percentage of macrophages outside the wells to be about equal to the percentage of projected surface area in between the wells, giving a value of one on the y-axis of the graph, as represented by the dotted line. However, for recessive topography ranging from 5-200 µm in size and 5-100 µm in spacing we see that all patterns have a ratio of percentage of macrophages in between wells to percentage of area in between wells

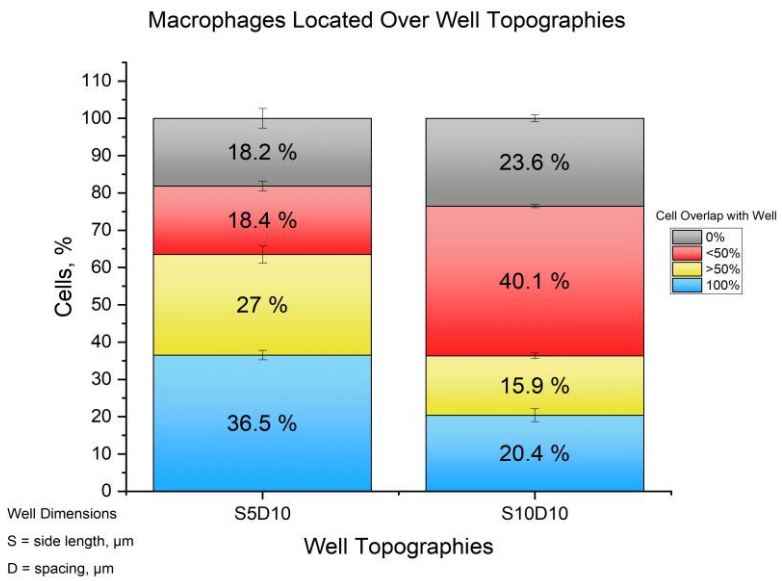

Figure 2: This graph reorganizes the data in Figure 1 to show more specifically how macrophages are located on the different well topographies for both 5x5 µm wells (left column) and 10x10 µm wells (right column). The colors show the how much of a well each cell is covering.

instances showing a statistically significant difference from the random distribution. This suggests that macrophages prefer interacting with recessive well topographies.

To look closer at macrophage preference for interacting with well topography, two-way ANOVA analysis was performed on macrophage position data from PDMS samples with recessive

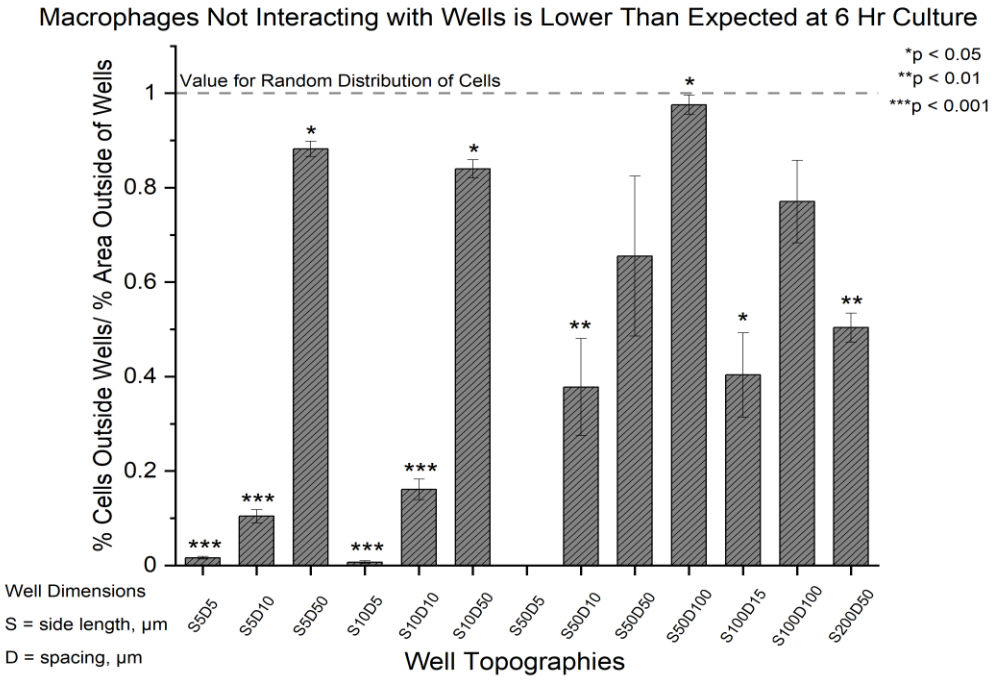

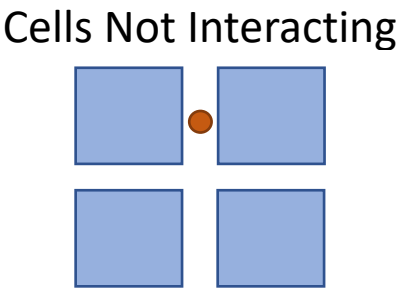

Figure 3: This graph compares macrophages that are not interacting with wells on various surface patterns. Each pattern has a projected surface area ratio that consists of well topography. Because of this, it can be assumed that a random distribution of macrophages would give a ratio of macrophages outside the wells equal to the percentage of macrophages on the surface (dotted line). Data contains at least 3 biological replicates for each sample and statistics is done by student's t-test comparison to random distribution value.

patterns of various side lengths and spacing. Both side length and spacing were seen to be statistically significant for affecting the localization of macrophage in or over well topography ($p<0.0001$). However, it

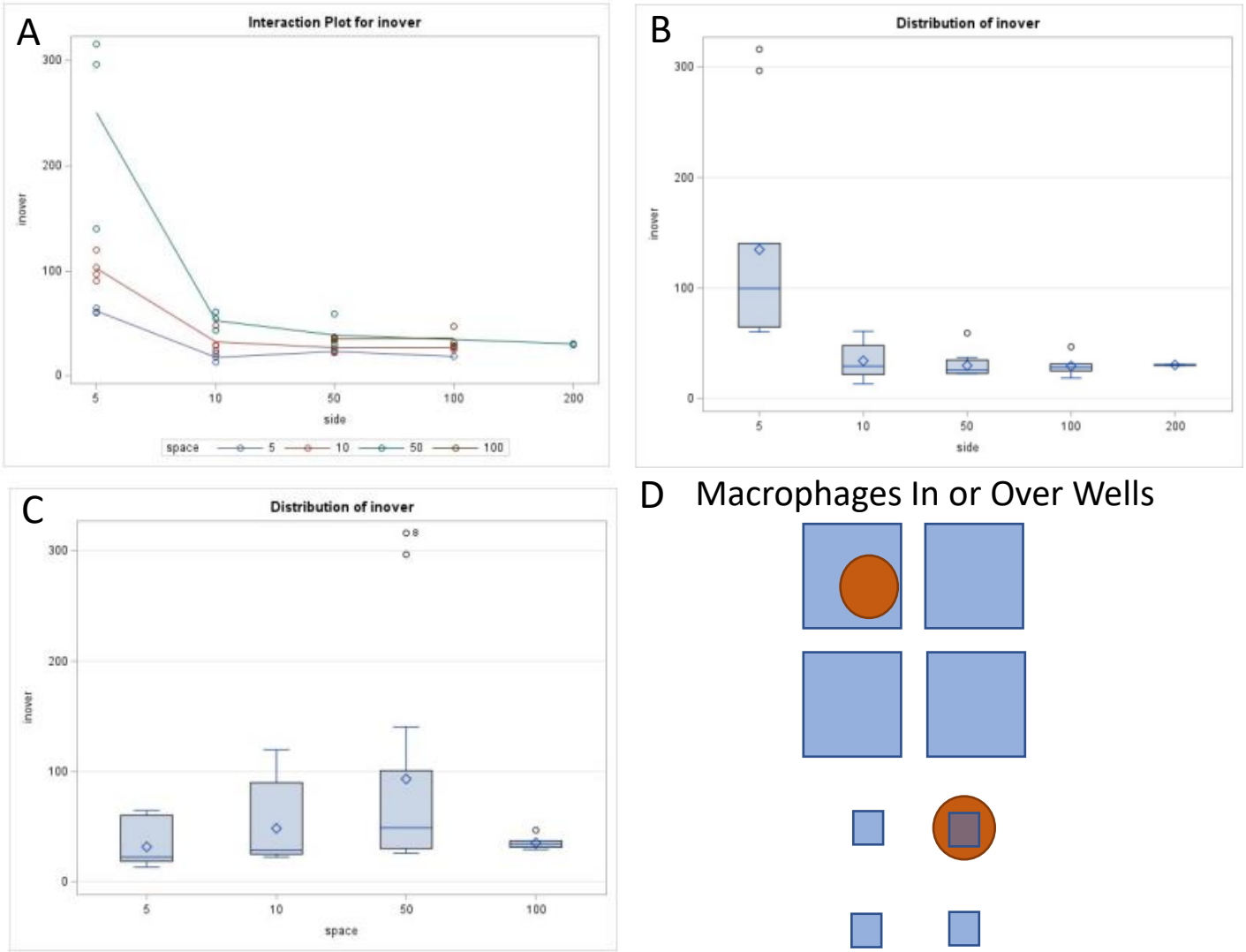

Figure 4: Macrophages over or inside wells, illustrated in (D), were analyzed. The interaction plot shows that increased spacing between wells biases more macrophages into wells for smaller wells (a). This may be an effect of lower well area on the patterns with increasing space. The box plot in (b) shows the means for macrophages in or over wells for each side length of well. The 5 µm side length mean was significantly different to all other side lengths ($p < 0.0001$, two-way ANOVA followed by Tukey test). The box plot in (c) shows the means for macrophages in or over wells for each well spacing. The 50 µm spacing was significantly different from all other spacings ($p < 0.0001$, two-way ANOVA followed by Tukey test). There were at least 3 biological replicates for each category compared.

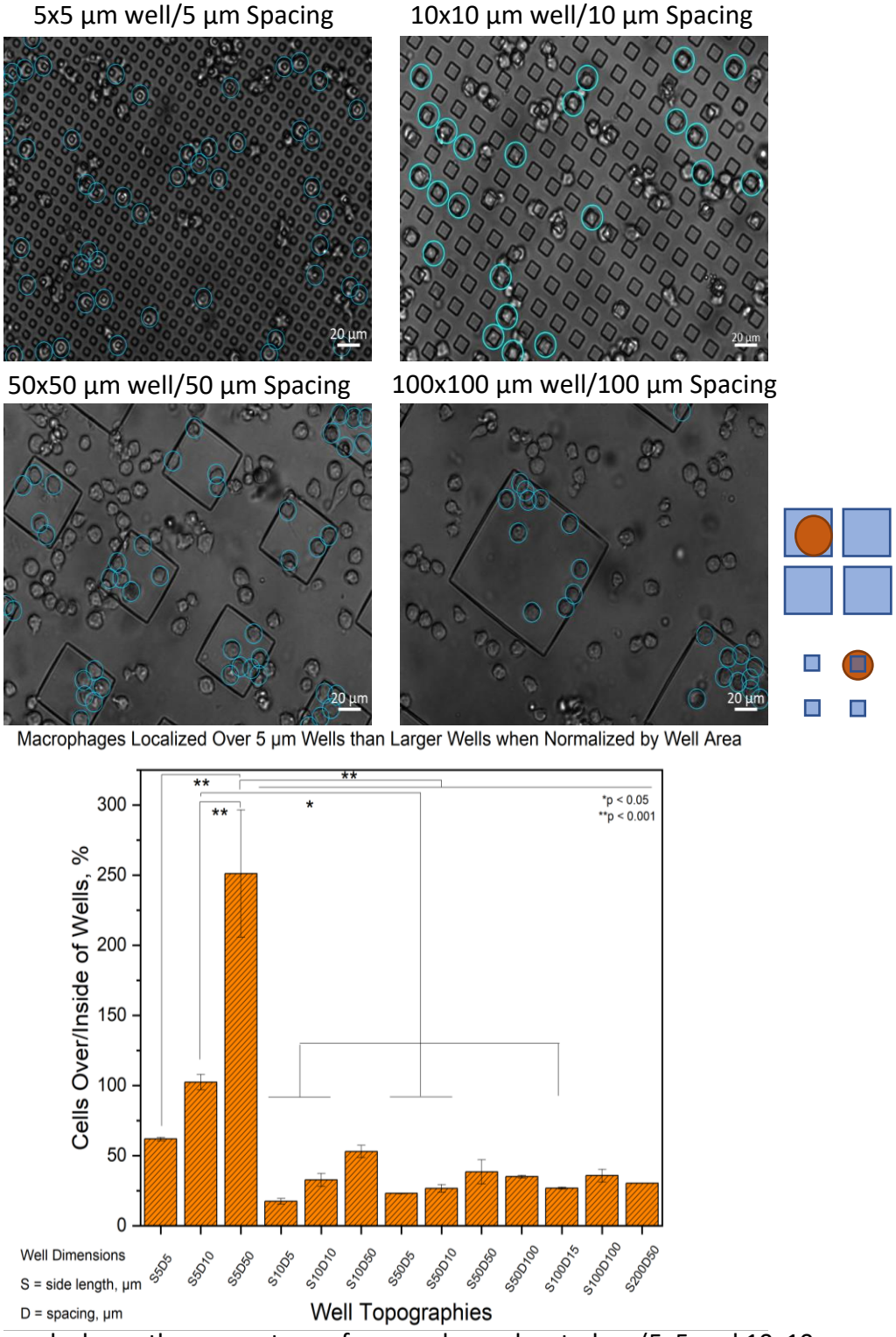

Figure 5: This graph shows the percentage of macrophages located on (5x5 and 10x10 µm wells) and inside (10x10 µm and larger wells) well topography normalized by the percentage of the surface that is comprised of wells. It is seen that there is an increased localization on wells with 5 µm side length. Images on the bottom represent data from some of the bars in the graph. Macrophages inside or over wells are circled in blue. Statistics with one-way ANOVA with Tukey test and at least 3 biological replicates per condition.

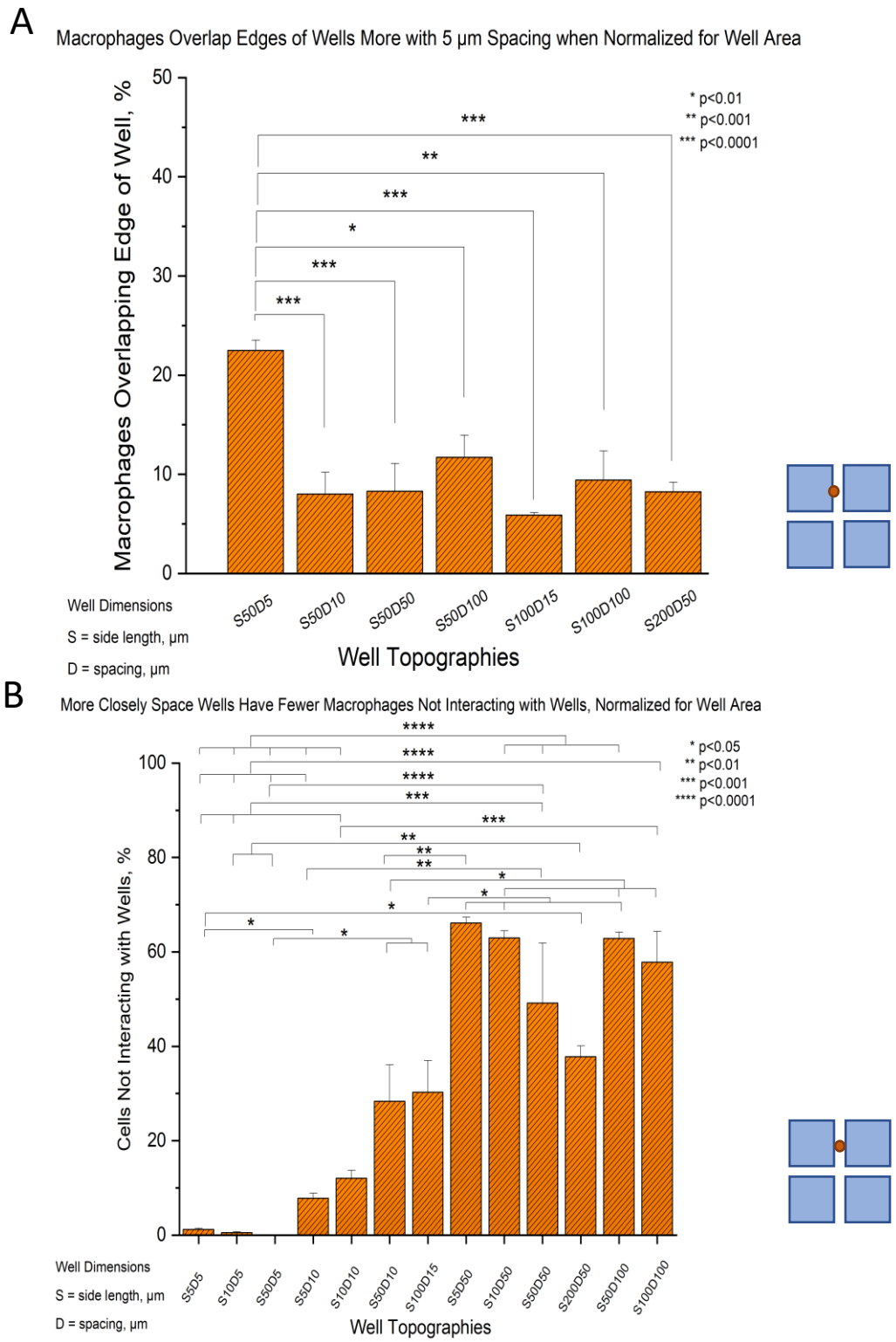

Figure 6: Graph A shows the percentage of macrophages overlapping the wall of well topography from outside the wells, while the Graph B shows the percentage of cells not interacting with well topography for patterns of various size and spacing. Both graphs are normalized by the area available for macrophages to occupy relative to the area available in the condition of the first bar. Statistics with one-way ANOVA with Tukey test and at least 3 biological replicates per condition.

was also seen that the interaction between these two independent variables was also significant ($p<0.0001$). Looking at the interaction plot in Figure 4A, it is seen that increased spacing between patterns leads to a bias in localization over wells at the 5 μm side length.

From here, one-way ANOVA was performed to check specific differences in localization over wells between patterns. The number of macrophages that were overlapping or inside of well patterns showed a preference for 5x5 μm wells compared to larger well sizes. This is most clearly seen when normalizing the data by the area of the wells available on each pattern (Fig. 5).

It was also observed that macrophages appear to prefer to overlap the walls of large wells, when the walls are only 5 μm wide, Figure 6A. It was also observed that macrophage could prefer interacting with wells that are more closely spaced, seen in Figure 6B. Further investigation would be needed to elaborate on these observations.

3.2 Macrophage Position in the Presence of Bacteria

Macrophage position was examined in the presence of E. *coli* to see if there would be a change in how macrophages interact with the topography. In Figure 7B, it is seen that there were fewer macrophages located over 5x5 μm wells in the presence of bacteria at 3 hours (26.1%), and at 6 hours (35.0%), compared to macrophage cultured alone for 6 hours (46.7%). For 10x10 μm wells, Figure 7A, fewer macrophages located in/over wells was also seen in the presence of bacteria for both 3 hours (12.0%) and 6 hours (12.2%) coculture compared to macrophages cultured alone for 6 hours (32.6%).

Because macrophage appear to prefer 5x5 μm wells and this preference appeared to decrease in the presence of bacteria, it was thought that maybe the bacteria outside of wells can distract macrophages away from interacting with the wells. To test this, we tested whether macrophage

A

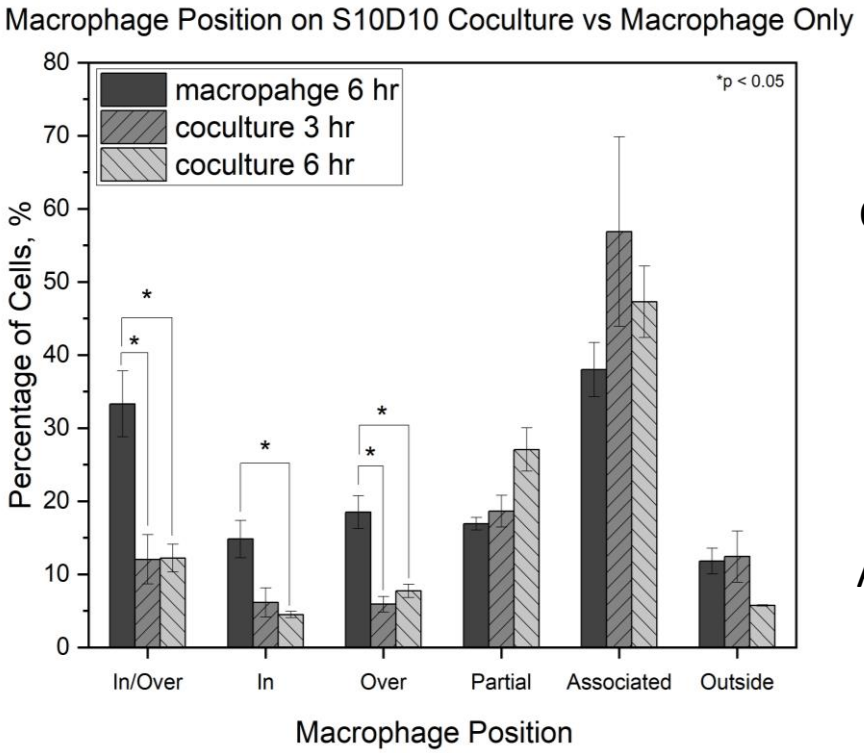

C

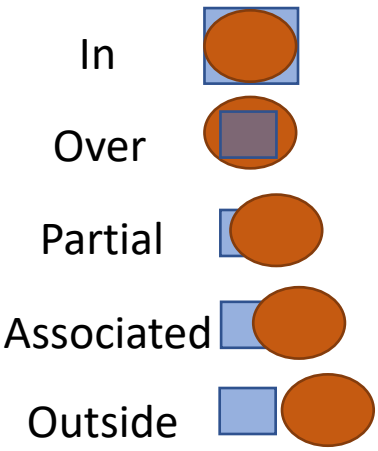

B

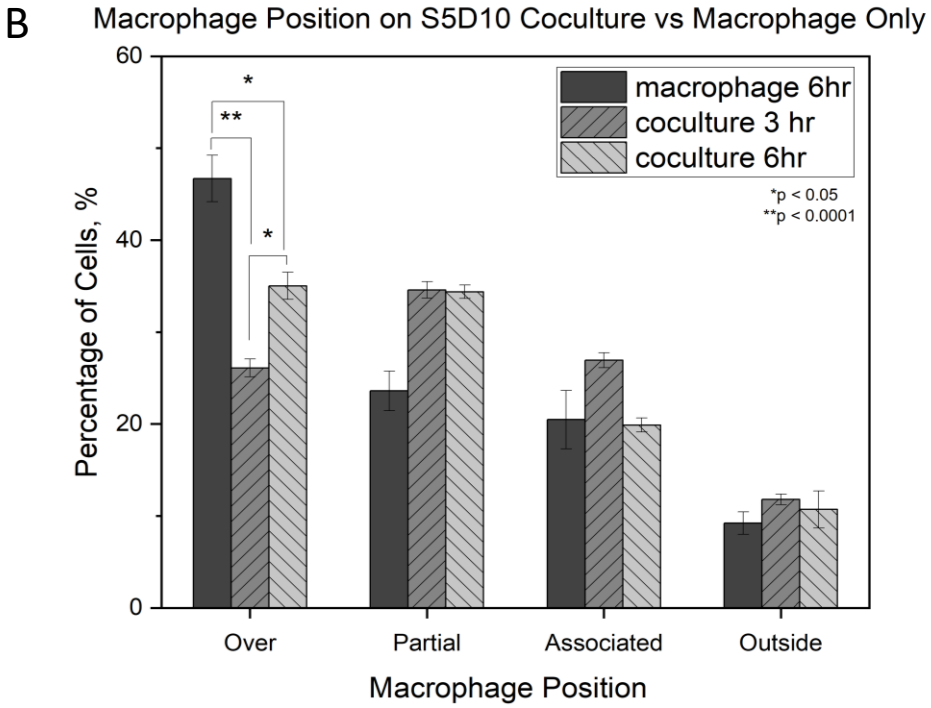

Figure 7: Graph A compares the macrophages position on well topography that has 10 µm side length and spacing for scenarios with only macrophages and the presence of E. *coli* RP437/pRSH103. Graph B makes the same comparison for wells with 5 µm side length and 10 µm spacing. The categories for macrophage position on the X-axes are indicated in diagram C. Statistics with one-way ANOVA with Tukey test and at least 3 biological replicates per condition.

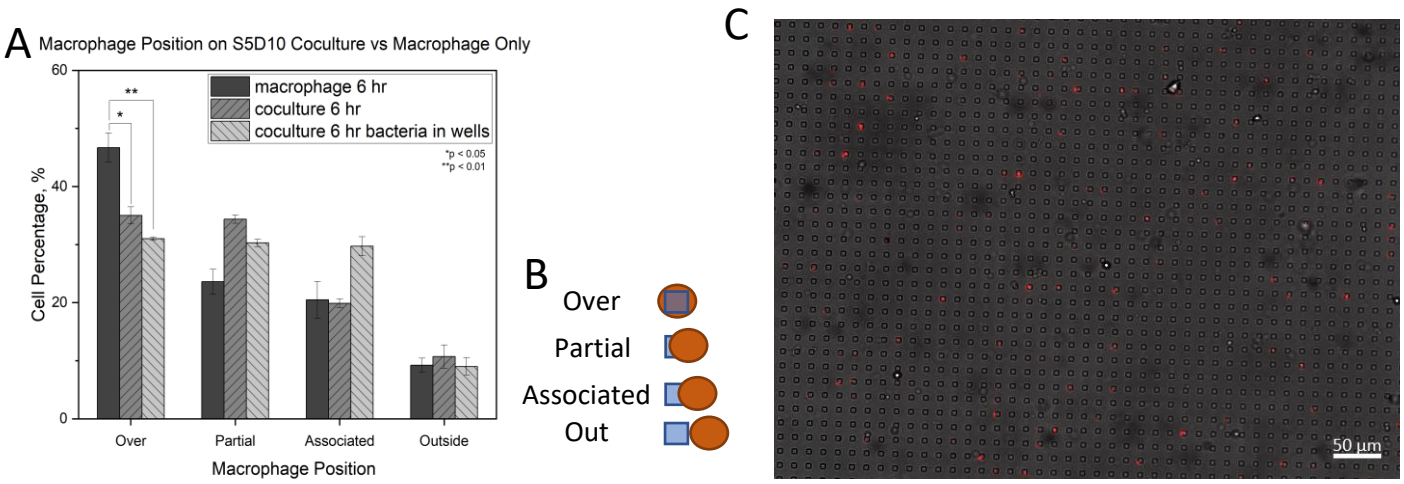

Figure 8: Graph A compares the macrophages position on topography that is 5 µm in side length and 10 µm spacing for scenarios with only macrophages and the presence of E. *coli* RP437/pRSH103, normal biofilm or with cells only in well topography. Image C shows an example of the sample surface when bacteria washed so that bacteria were only left in the recesses of the topography. The categories for macrophage position on the X-axis are shown in diagram B. Statistics with one-way ANOVA with Tukey test and at least 3 biological replicates per condition.

position would be different if bacteria were only inside the wells of the topography. This was done by rubbing the surface of the biofilm to shear away any bacteria not in the wells of the surface. An example of this is seen in the image in Figure 8C. Figure 8A also shows that there was not much change in the decrease of macrophage localization on wells with regular biofilm compared to biofilms with bacteria only in the wells. This suggests that the presence of bacteria, regardless of their position, is enough to decrease the tendency for macrophages to l located over well-shaped topography. The cause behind this is not clear and further study with higher concentration of bacteria in wells may give different results because the processing of the sample to remove bacteria outside of wells also removed a lot of bacteria inside the wells. This left many wells without bacteria, which could diminish any effect of bacteria presence in wells on macrophage location.

3.3 Macrophage Movement Observations

Macrophage movement was observed and tracked on flat and pattern surfaces. Preliminary data showed that macrophages appear to move more on flat surfaces than 5x5 µm wells within the first 2 hours after inoculation, as seen in Figure 9A,B where there are longer tracks on the flat surface compared to the patterned surface. It was observed that macrophages tend to hop from well to well on 5x5 µm wells, example in Figure 9C,D, whereas they move more continuously on flat surfaces. It was observed that a macrophage can persist for up to 15 min on a well before hopping to the next. This provides evidence that patterned topography may limit macrophage movement, which could make phagocytosis less effective if macrophages cannot chase bacteria as well on these surfaces.

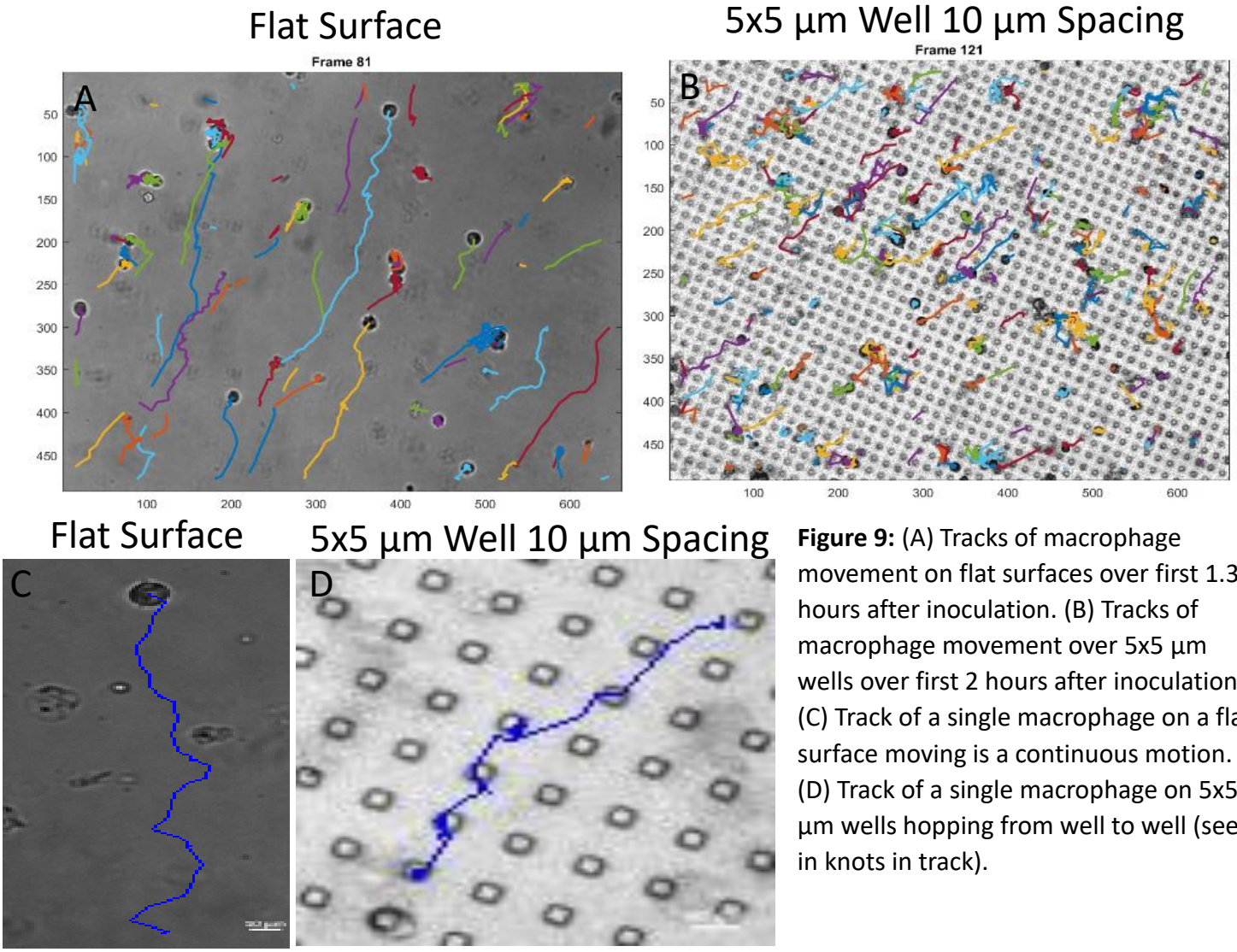

Figure 9: (A) Tracks of macrophage movement on flat surfaces over first 1.3 hours after inoculation. (B) Tracks of macrophage movement over 5x5 µm wells over first 2 hours after inoculation. (C) Track of a single macrophage on a flat surface moving is a continuous motion. (D) Track of a single macrophage on 5x5 µm wells hopping from well to well (seen in knots in track).

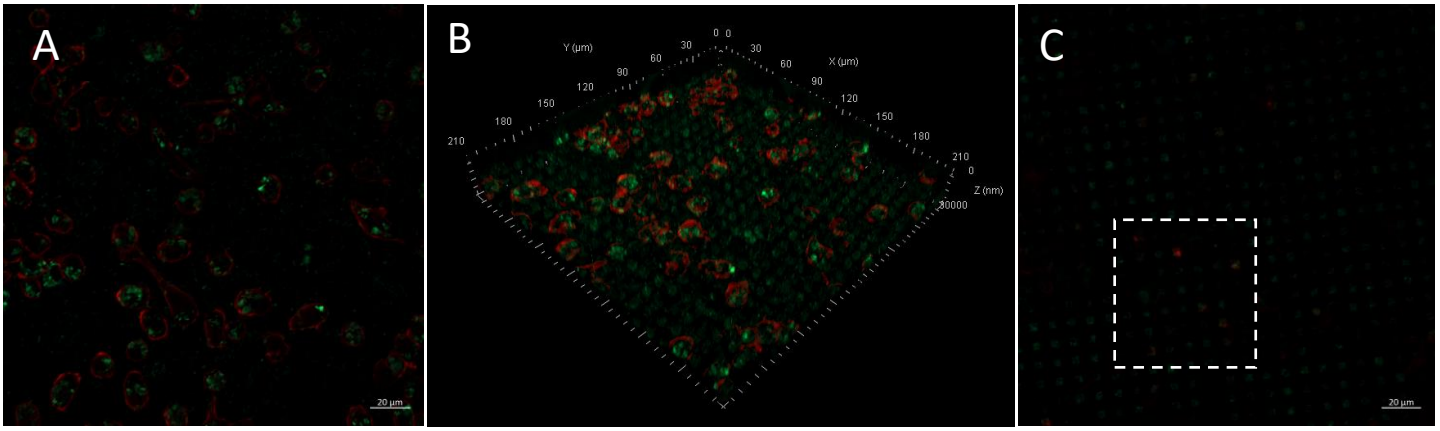

Figure 10: Macrophages (Red) on 5x5 µm wells after 3 hours coculture with E. *coli* (Green). Left – 2D image in main plane of macrophages, Middle – 3D image of 5x5 µm well surface, Right – Cross-section of z-stack in plane 5x5 µm wells showing bacteria in wells, dotted lines highlights a region with macrophages reaching into wells. Macrophages – actin phalloidin stain, E. coli – pGLO GFP

3.4 Phagocytosis on Pattern Surfaces

For a qualitative understanding of macrophage and bacteria interaction on recessive topography, z-stacks were taken after 3 hours of coculture to see if macrophages could reach down into small well topography. Macrophages were seen to reach down into 5x5 µm wells (Figure 10C), showing that bacteria inside of small wells may still be susceptible to phagocytosis. Figure 11 shows a zoomed in subset from the images in Figure 10. When the z-stack is looked at from the side in image C of Figure 11, it is seen that a lot of the bacteria are in the wells in green, while there are also some macrophages reaching into the wells. Image D from Figure 11 shows the bacteria and macrophage channels separated, and depth coded, to show the height of the cells. It is seen that both the macrophages and bacteria reach to about the same depth in the topography, demonstrating that macrophages can reach into 5x5 µm wells to interact with bacteria.

Even though macrophages may be able to reach into wells and phagocytose bacteria, the tight space may still make it difficult for phagocytosis to occur. To better understand this, phagocytosis was quantified on different surface topographies. Flow cytometry results in Figure 12 showed that a larger percentage of macrophages had phagocytosed bacteria after 3 hours on

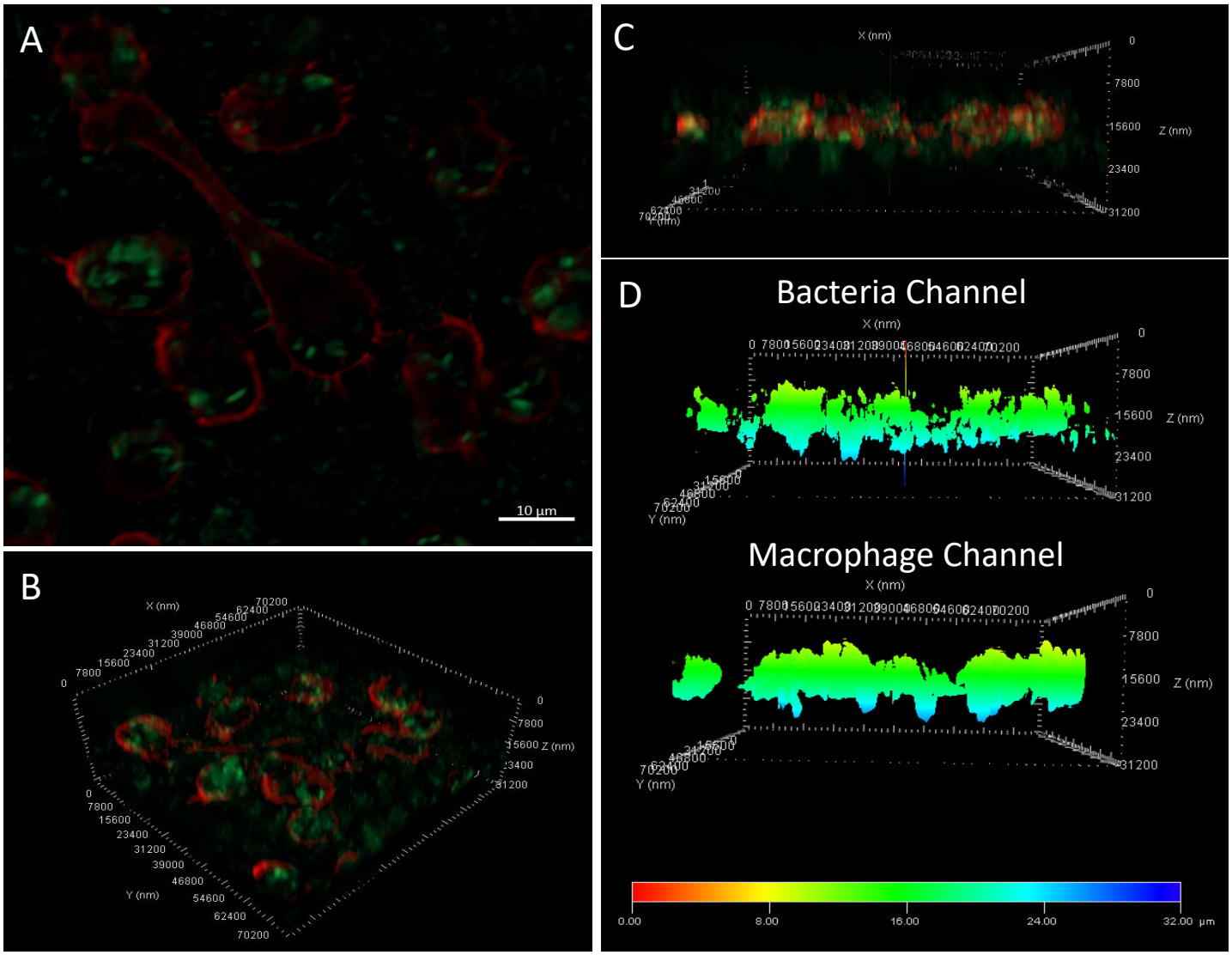

Figure 11: 2D image of macrophages (Red) and E. coli (Green) after 3-hour coculture (a). 3D image of macrophages and E. coli after 3-hour coculture (b). Side view of macrophages and E. coli showing bacteria presence in wells (green rectangles below the plane of macrophages) and some macrophages reaching into wells (c). Depth encoded side views of macrophage (top) and bacteria (bottom) channels showing that both macrophages and bacteria reach down to about the same depth in 5x5 µm wells (d). Macrophages – actin phalloidin stain, E. coli – pGLO GFP

either 5x5 or 50x50 µm wells than on flat surfaces. It was realized that a much larger quantity of bacteria per macrophage is present on the pattern surfaces compared to the flat surfaces, 3.4:1 for flat surfaces, 7.1:1 for 50x50 µm wells with 10 µm spacing, and 18.6:1 for 5x5 µm wells with 10 µm spacing. This may be the reason a larger percentage of macrophages were seen to phagocytose bacteria on patterns in flow cytometry.

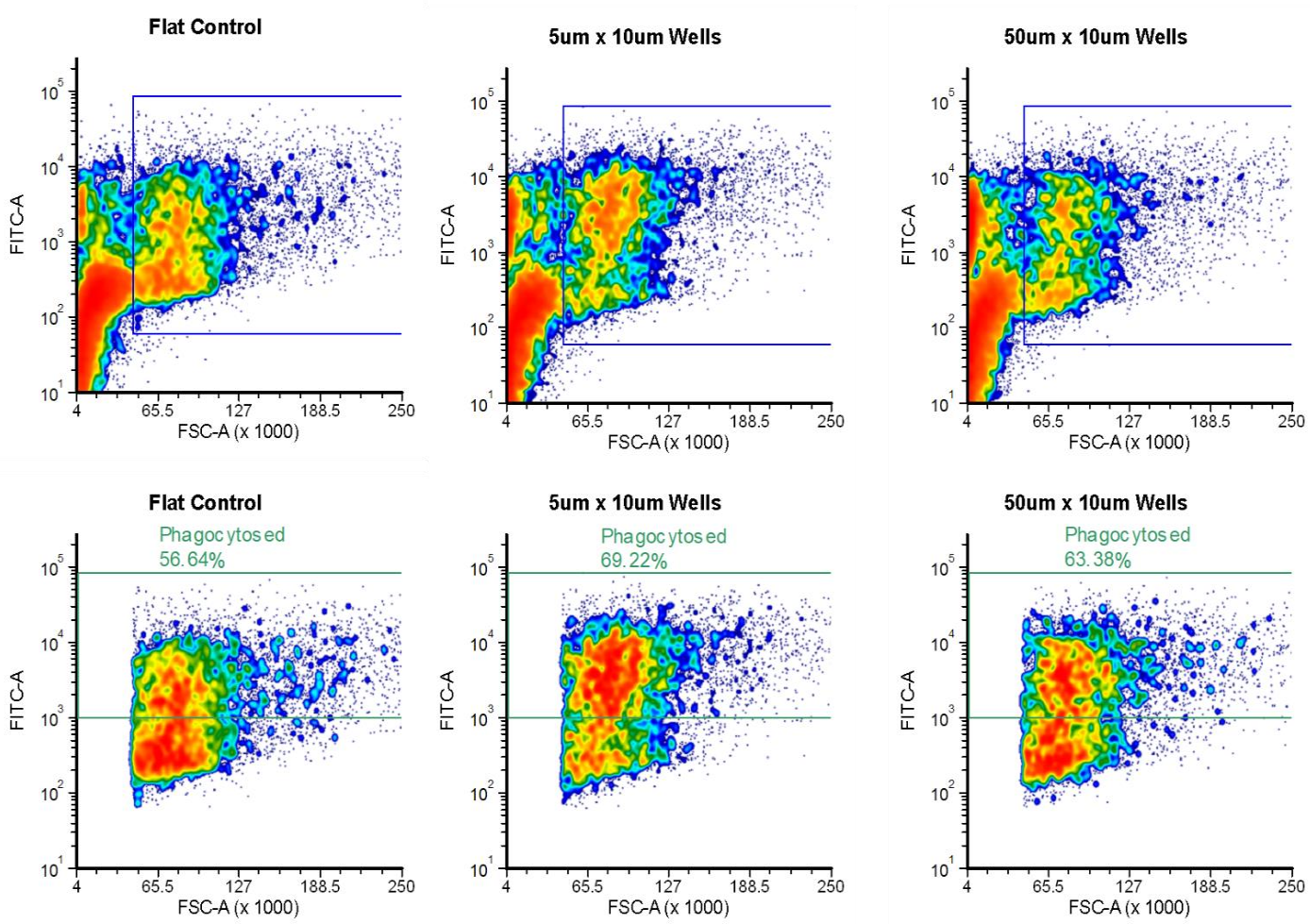

Figure 12: Flow cytometry comparison of percentage of macrophages that phagocytosed bacteria after 3 hours coculture. Flow cytometry was done on flat (left graphs), 5x5 µm wells (middle graphs), and 10x10 µm wells (right graphs). The top graphs show the gated regions for macrophages based on size along the x-axis, where particles outside of the gate should be bacteria and debris. The bottom graphs show the macrophage population gated again by fluorescence to show the percentage of macrophages that have phagocytosed bacteria. Cells from 4 biological replicates were combined to achieve cell numbers for flow cytometry.

To account for differences in bacteria-to-macrophage ratio seen on these samples, phagocytosis was also quantified by counting the bacteria inside of macrophages after 3 hours of coculture. The data was then normalized by the bacteria-to-macrophage ratio in the images. Figure 13A shows that more bacteria are present in macrophages on patterned surfaces compared to flat surfaces before normalizing for bacteria-to-macrophage ratio. Also, before normalization, Figure 13A, 2x2 μm wells showed lower phagocytosis like flat surfaces, which may be because there were a little to no bacteria or macrophages reaching into these wells. The bacteria-to-macrophage ratio for these different patterns were seen to vary drastically between flat surfaces and recessive patterns, which may explain why there is more phagocytosis per macrophage on these surfaces. To account for this, Figure 13B shows a graph where the phagocytosis data is linearly normalized to a 10:1 bacteria-to-macrophage ratio. When this normalization is applied, it is seen

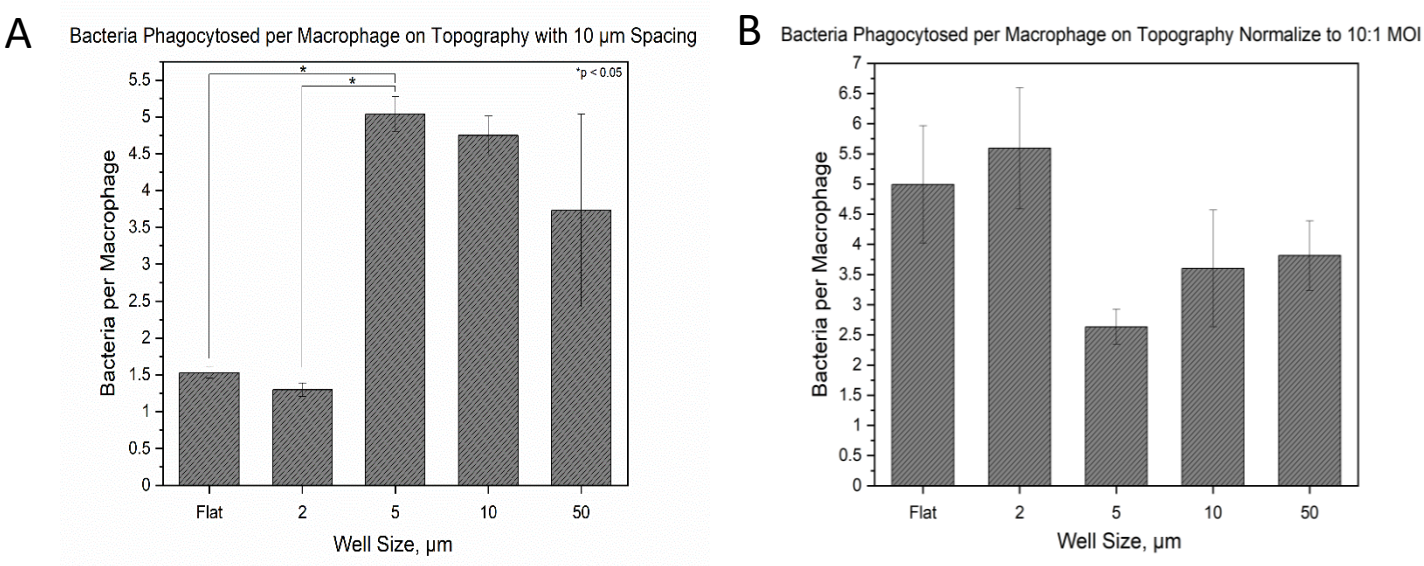

Figure 13: These graphs show macrophage phagocytosis counted by bacteria per macrophage on 10 μm deep wells after 3 hours of coculture. The left graph shows more bacteria phagocytosis per macrophage on pattern surfaces. However, the right graph shows the same data linearly normalized to account for the variation in bacteria to macrophage present on the surface (MOI 10:1), demonstrating that 5x5 μm wells may lead to less phagocytosis by macrophages than on flat surfaces. Statistics with one-way ANOVA with Tukey test and at least 3 biological replicates per condition.

Macrophages on 30 um Deep Wells 2 µm wide

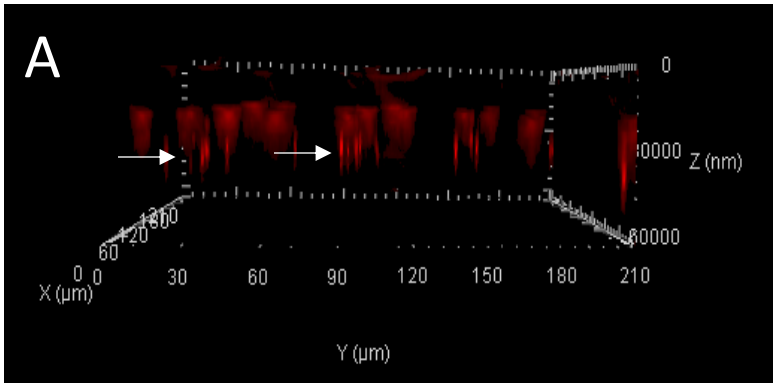

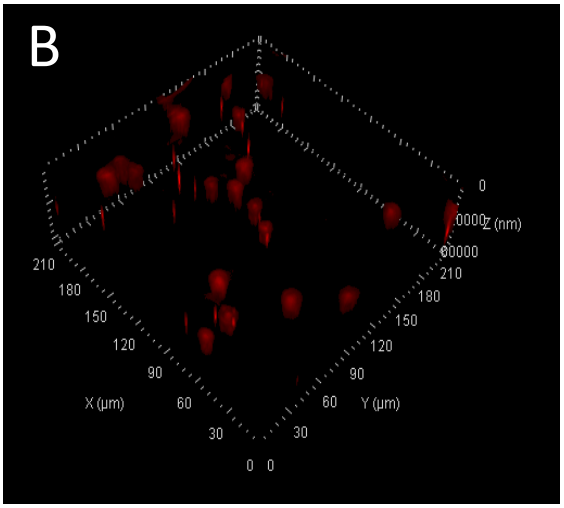

Coculture on 30 um Deep Wells 2 µm wide

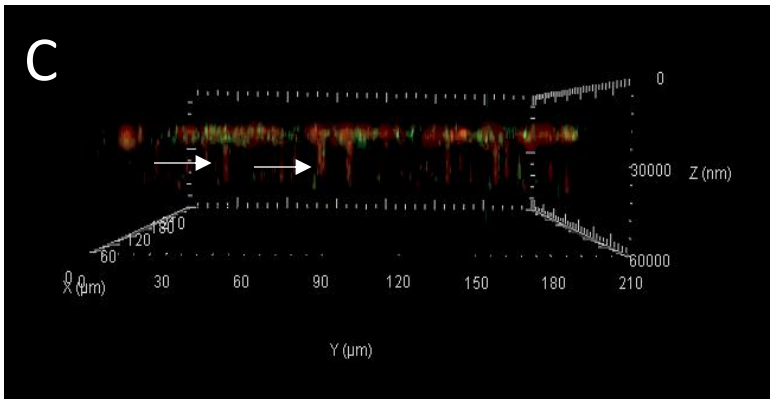

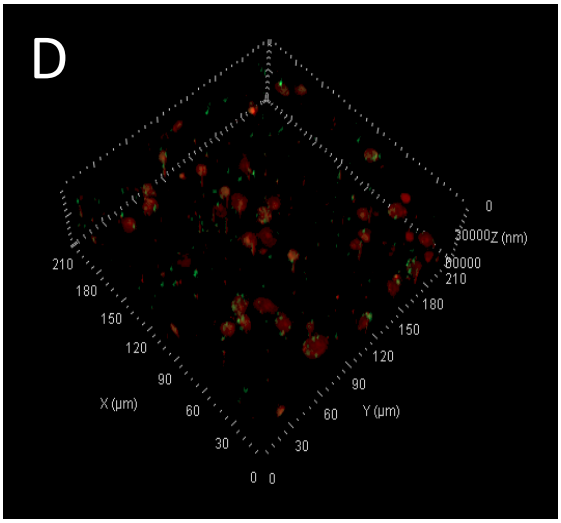

Macrophages on 30 um Deep Wells 10 µm wide

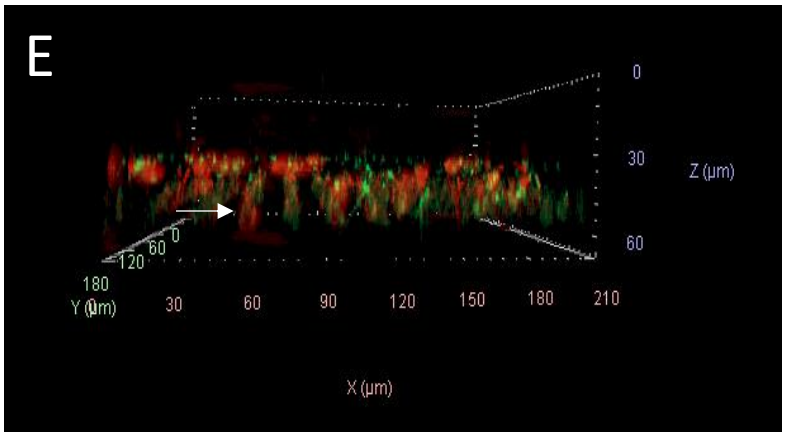

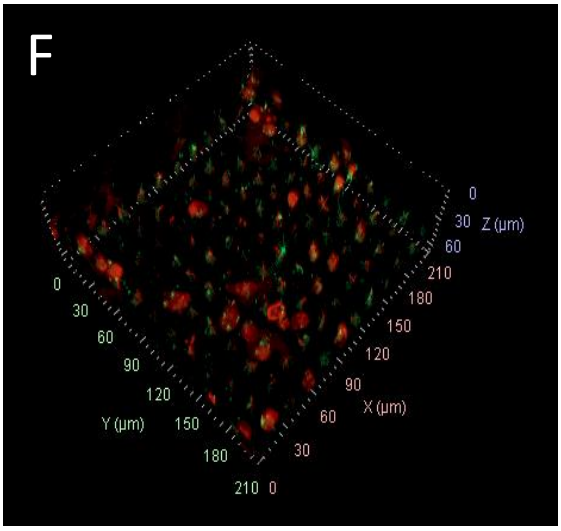

Figure 14: A,B – Macrophages cultured on 2 µm wide, 30 µm deep wells. C,D – Coculture of macrophages and E. coli on 2 µm wide, 30 µm deep wells. E,F – Coculture of macrophages and E. coli on 10 µm wide, 30 µm deep wells. White arrows show macrophages reaching into wells. Macrophages in red, stained with propidium iodide, and E. coli in green with GFP.

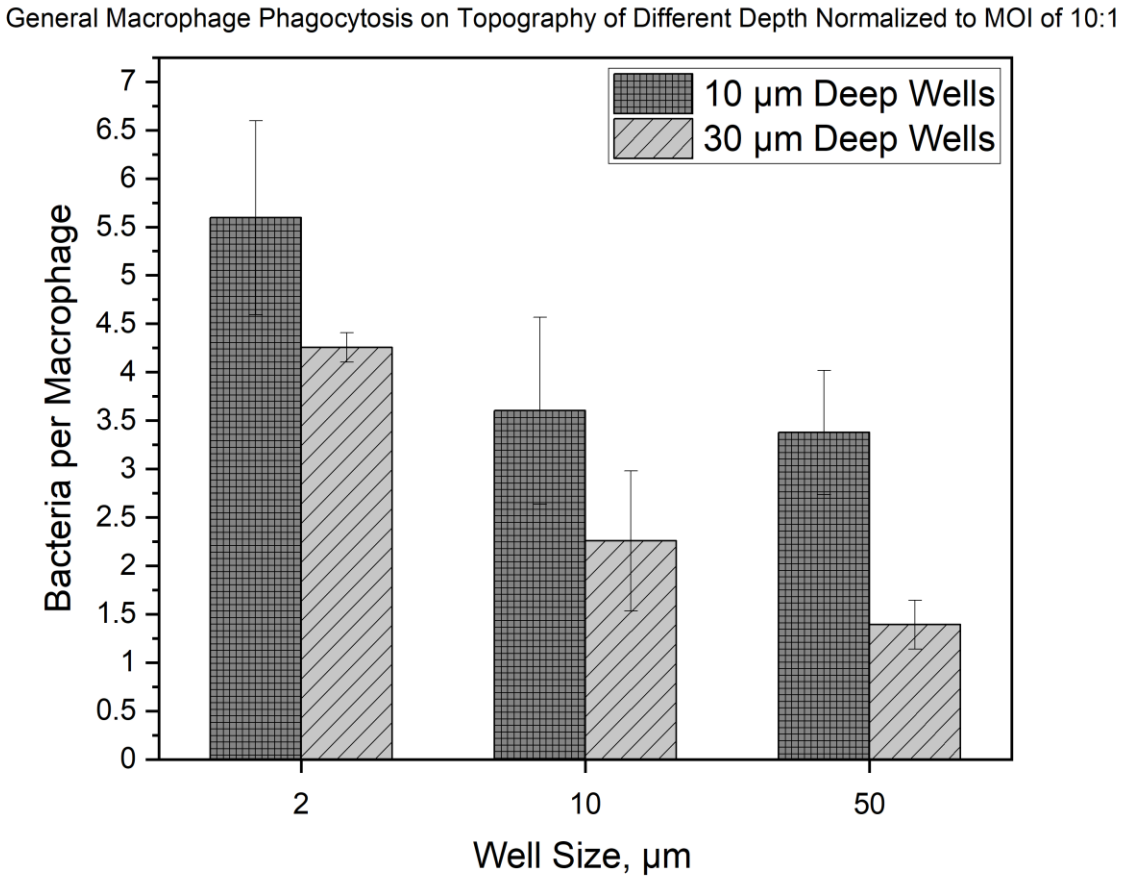

Figure 15: This graph shows the amount of E. coli in each macrophage when cocultured on topographies of different depths. After normalizing for differences in bacteria-to-macrophage ratio, it is seen that there is less phagocytosis on deeper 30 µm wells than 10 µm wells. Statistics with one-way ANOVA with Tukey test and at least 3 biological replicates per condition.

that there is more phagocytosis on the flat surface compared to the 5x5 µm wells, which suggests that there is a limitation of phagocytosis on 5x5 µm wells that are 10 µm deep.

Macrophages were also studied on recessive patterns that were 30 µm deep. Figure 14 shows 3D images of macrophages and bacteria on 30 µm deep wells. It was seen that macrophages will squeeze deep into 2x2 µm wells this deep with or without bacteria present. This was also seen for larger wells, that were 10x10 µm deep.

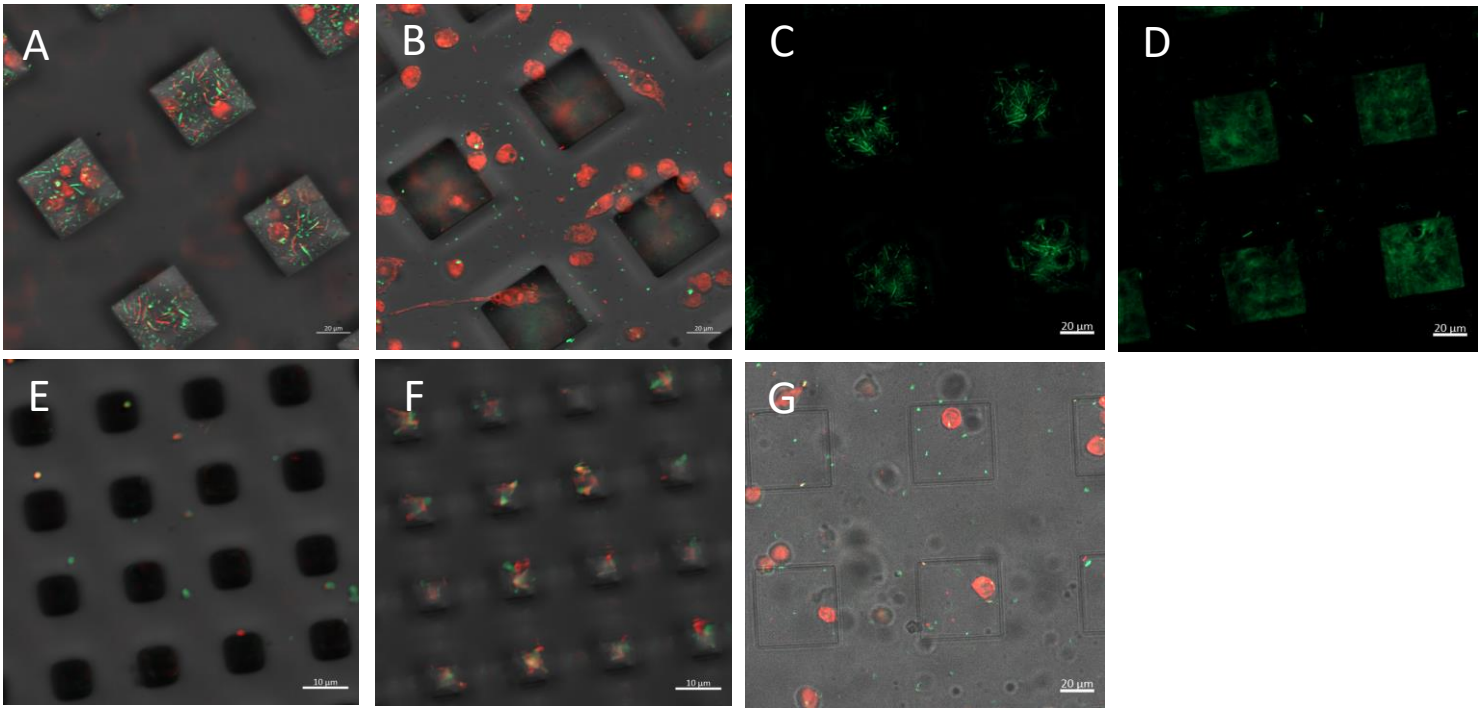

Figure 16: Then E. *coli* (green) were cocultured with macrophages (red) on 30 µm deep wells, 50 µm wide, it was seen that bacteria at the bottoms of the wells filament (a), whereas those at the tops of the wells do not (b). When E. *coli* was cultured alone on 30 µm deep wells, filamentation was still seen at the bottom (c), but not the top of the wells (d). When bacteria are cocultured on 30 µm deep wells with 10 µm wide, some degree of filamentation is seen in the bottoms of the wells (e), but not the top (f). E. *coli* cocultured on 10 µm deep wells of similar size, did not show filamentation (g). Macrophages in red stained with actin phalloidin stain. E. coli in green with plasmid expressed GFP.

Phagocytosis data on 30 µm deep topography and 10 µm deep topography suggests that the depth of the topography may limit phagocytosis of bacteria. Figure 15 shows that, when normalized to a bacteria-to-macrophage ratio of 10:1, macrophages on 2x2 µm, 10x10 µm, and 50x50 µm wells had more bacteria in them after 3 hours of coculture on 10 µm deep wells than 30 µm deep wells. This implies that bacteria may be protected from phagocytosis in deep pockets on the surface.

Further, it was noticed that bacteria filamented at the bottoms of 50x50 µm wells with and without the presence of macrophages (Figure 16 A, B, C, D). This was also seen to a lesser degree in 10x10 µm wells, 30 µm deep (Figure E, F). Filamentation was not seen in wells that were 10 µm deep (Figure 16 G). Filamentation may be a reason for decreased phagocytosis on 30 µm deep wells compared to 10 µm deep wells, especially since the difference in phagocytosis between 10 µm and 30 µm deep wells appears to increase with size (Figure 15), which matches the filamentation seen in Figure 16. To further support this, Figure 17 shows that the number of

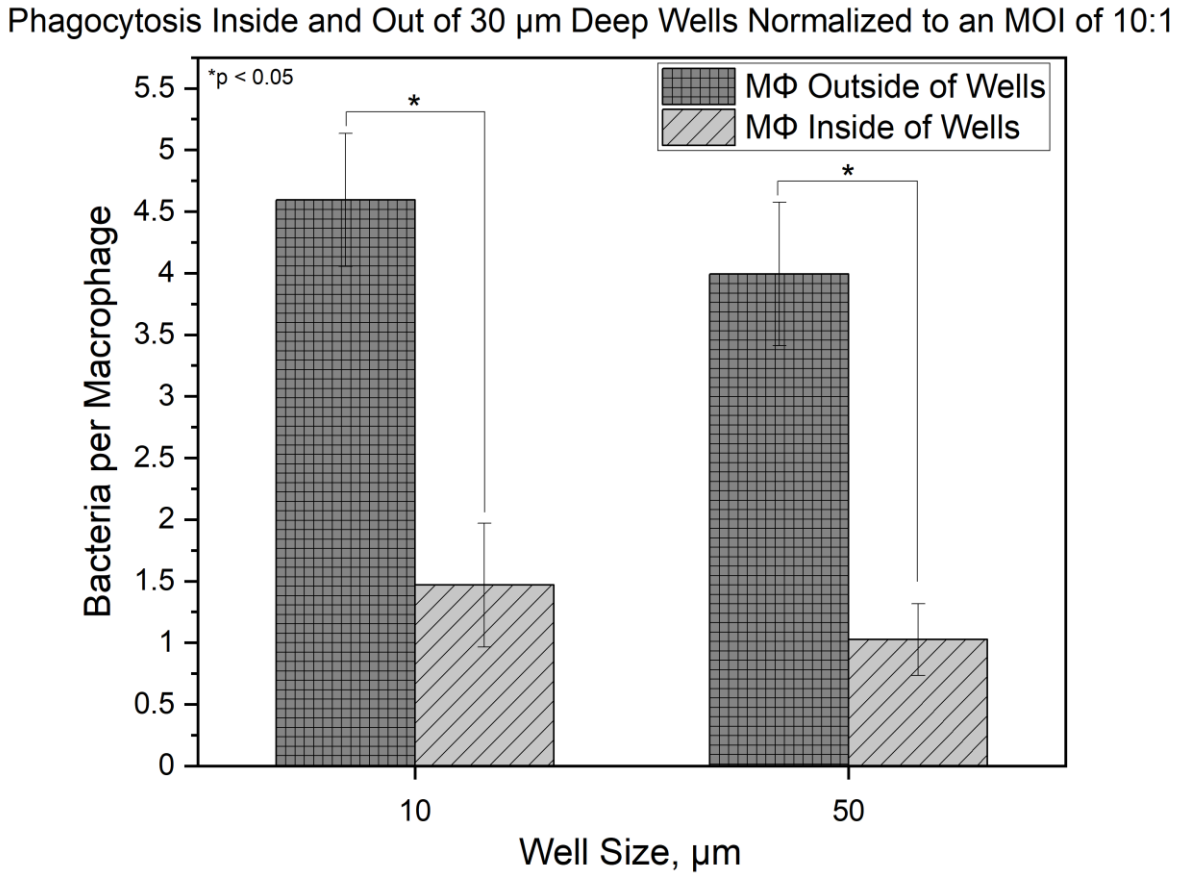

Figure 17: This graph shows the difference in phagocytosis between macrophages inside of 30 µm wells and outside of 30 µm wells, normalized to account for differences in bacteria-to-macrophage ratio in and out of the wells. This data shows limited phagocytosis inside of the wells. Statistics with one-way ANOVA with Tukey test and at least 3 biological replicates per condition.

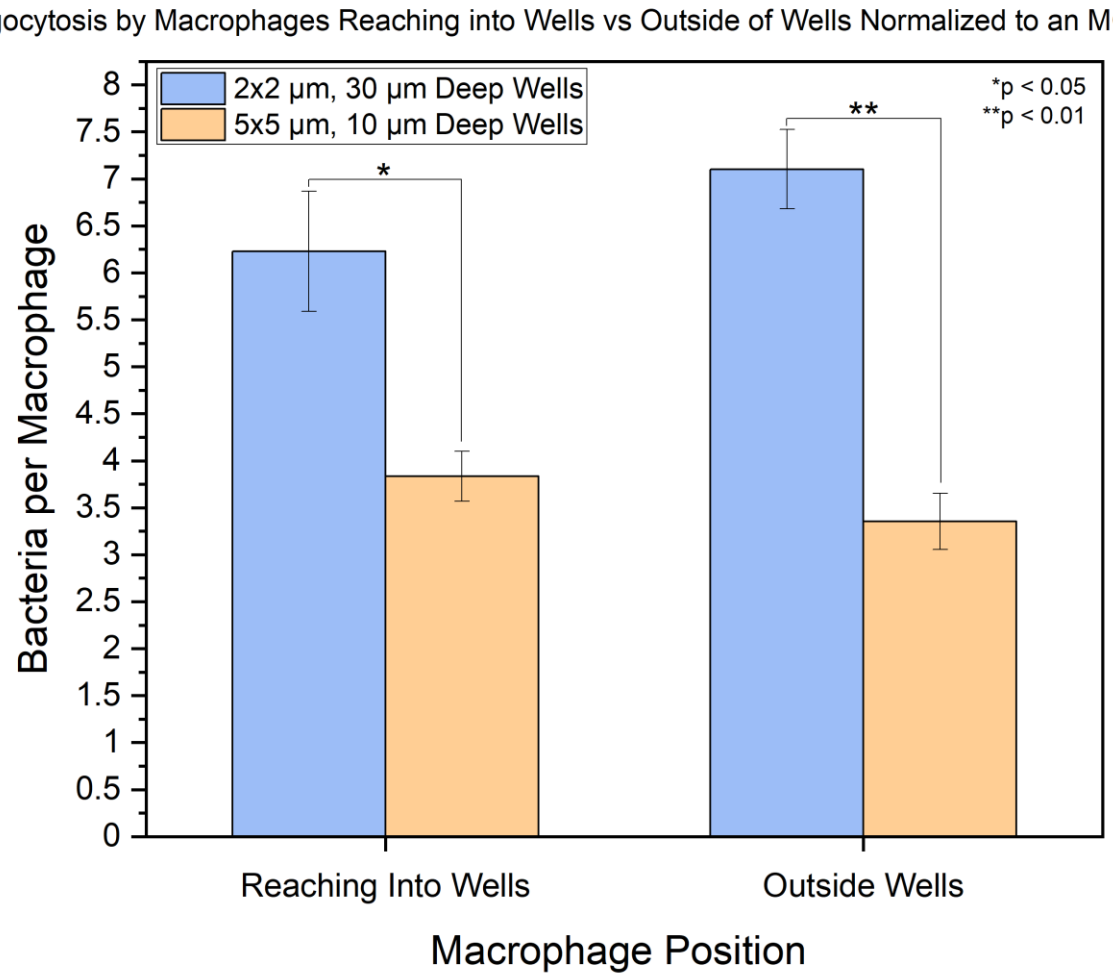

Figure 18: This graph shows the difference in phagocytosis between macrophages reaching into small wells and not reaching into wells after normalizing for differences in bacteria-to-macrophage ratio. It is seen that macrophages reaching into smaller, deeper wells phagocytose more than those reaching into slightly larger, shallower wells. This contradicts other data suggesting that smaller and deeper wells might decrease phagocytosis, but is should also be acknowledged that phagocytosis on the smaller, deeper well pattern in general was higher regardless of reaching into wells, which suggests another factor may justify the difference in phagocytosis. Statistics with one-way ANOVA with Tukey test and at least 3 biological replicates per condition.

bacteria per macrophage is higher for macrophages outside of wells compared to macrophages inside of wells on 30 µm deep topography when normalized to account for the difference in bacteria-to-macrophage ratio. These data support the notion that deeper topography discourages phagocytosis of bacteria.

In opposition to this, the graph in Figure 18 shows a comparison of phagocytosis for macrophages reaching into 30 μm wells and 10 μm wells vs macrophages on these samples not reaching into the wells. This data shows macrophages reaching into smaller and deeper, 2x2x30 μm, wells phagocytose more bacteria than those reaching into larger and shallower, 5x5x10 μm, wells. While this data goes against the previous data suggesting that small and deep wells limit phagocytosis, it should be noted that macrophages not reaching into the smaller 2x2x30 μm wells also phagocytosed considerably more than those not reaching into the 5x5x30 μm wells. This suggests that there may be another factor influencing phagocytosis on these samples. For example, maybe the 5x5 μm well is more of a distraction, than 2x2 μm wells, from phagocytosing bacteria on the surface outside of the wells, since macrophages reaching into these small wells tend to be mostly outside of the well.

Lastly, it can be noted in to Figure 18 that this is a small decrease in phagocytosis for 2x2x30 μm wells between macrophages reaching into the wells and those not reaching in. This is in opposition to 5x5x10 μm wells were macrophages reaching into wells phagocytose slightly more than those not reaching in. This provides small evidence that reaching into the smaller and deeper wells imposed at least a little limitation on phagocytosis.

4. Discussion

Previous work has shown that nanotextured surfaces on implants can lead to bacteria death[29]. Micro-topographies, on the other hand, give a more mixed results where biofilm formation may be reduced[30], but certain topographic features, such as in valley between micropillars[31], may promote bacteria accumulation. In the case of textured breast implants certain topographies were seen to accumulate more bacteria and are linked to cancer[14,15], which may be the result of

chronic infection. This works seeks to improve the understanding of how macrophages and macrophage phagocytosis are affected by micron scale recessive topographies, which could give insight into how these topographies effect bacteria removal from a surface by the immune system.

In this work we found that there is a general preference for macrophages to interact with recessive topography (Figure 3). This was especially the case for 5x5 μm wells, where localization on wells appeared to be the highest (Figure 5). This is similar to a study in the literature that found macrophage attachment preferential for pillars below 10 μm in width, with 5 μm-scale pillars evoking the strongest response[21]. It seems that this 5 μm-scale may trigger some response in macrophages that causes concentration to these areas with these features. It would be interesting to see if this is related to an immune response to the surface, such as frustrated phagocytosis of the topography, or some mechanism associated with improved mechanical attachment.

Strangely, when bacteria were already present on the surface, it was seen the macrophage localization over well topography decreased (Figure 7). This was even the case for scenarios where bacteria were only inside of the well topography (Figure 8). It may be possible that the presence of bacteria in the wells creates some sort of signal that discourages macrophages from fully overlapping the wells. Maybe biofilm presence in the wells makes it more difficult for macrophages to attach in the wells. Further work would be needed for a solid explanation of this phenomenon.

The phagocytosis results show some evidence for decreased phagocytosis on small wells of 5x5 μm (Figure 13), which suggests that certain topography could have a negative effect on

phagocytosis. Further, a lot of the recessive topographies were seen to have a much larger bacteria presence, which could also discourage clearance of an infection in vivo. Phagocytosis is decreased on 30 μm deep topography compared to 10 μm deep topography (Figure 15), suggesting that these deeper pockets protect bacteria more. This is further supported by the decrease in phagocytosis by macrophages in 30 μm deep wells compared to those outside of the wells (Figure 17). Bacteria were seen to filament at the bottoms of 30 μm deep wells (Figure 16), which may be a cause for the decrease in phagocytosis on these surfaces. It has been seen in the literature that when macrophages approach a filamented bacteria they must reorient to the pole of the bacteria to start phagocytosing it, which could take 70 min[36]. This suggests that microtopographies that create deep pockets, especially pockets that are large enough to allow for bacteria filamentation, could slow down phagocytosis of bacteria.

5. Conclusions and Future Work

The recent recall on breast implants associated with BIA-ALCL and its possible link to chronic device infection highlights the importance of how device surfaces interact with pathogens. If topography on a device surface can protect bacteria from phagocytes, then it could lead to long-term inflammation that could trigger cancer formation. The results and observations from this study suggest that certain microtopographies effect macrophage behavior, such as their positioning and movement. Evidence for changes in the effectiveness of phagocytosis were also seen on well topographies of different sizes and depths. Notably macrophages appear to elicit the strongest reaction from 5 um-scale topography, with a high tendency for cells to locate on wells and possibly lead to a decrease in phagocytosis. Further, 30 μm deep wells appear to create a decrease in phagocytosis, which may be associated with the promotion of filamentation at the bottom of 30 μm deep wells. Overall, these results create an initial understanding of how

microtopographies may influence macrophage behavior and phagocytosis of microbes, which could provide insights for how more complicated topographies could protect biofilms from the immune system.

Future work could look at the biological changes within the macrophages that are located on 5 μm scale topography to obtain a better understanding of the phenomena and understand if these surfaces are encouraging a particular macrophage phenotype. It would also be interesting to move forward with more complicated topographies, such as the porous surfaces seen on textured breast implants. It is possible that deep pores on these surfaces encourage bacteria filamentation or limit macrophage surface exploration by encouraging localization on topographic features. These studies could further our understanding of how surface topographies on medical devices might limit removal of infectious pathogens, and how to avoid such features to engineer safer devices.

References

1. CDC. (2022, March 17). *Antibiotic Resistance Threatens Everyone*. Centers for Disease Control and Prevention. https://www.cdc.gov/drugresistance/index.html
2. Høiby, N., Bjarnsholt, T., Givskov, M., Molin, S., & Ciofu, O. (2010). Antibiotic resistance of bacterial biofilms. *International Journal of Antimicrobial Agents*, *35*(4), 322–332. https://doi.org/10.1016/j.ijantimicag.2009.12.011
3. Magana, M., Sereti, C., Ioannidis, A., Mitchell, C. A., Ball, A. R., Magiorkinis, E., Chatzipanagiotou, S., Hamblin, M. R., Hadjifrangiskou, M., & Tegos, G. P. (2018). Options and Limitations in Clinical Investigation of Bacterial Biofilms. *Clinical Microbiology Reviews*, *31*(3). https://doi.org/10.1128/CMR.00084-16
4. Elinav, E., Nowarski, R., Thaiss, C. A., Hu, B., Jin, C., & Flavell, R. A. (2013). Inflammation-induced cancer: Crosstalk between tumours, immune cells and microorganisms. *Nature Reviews. Cancer*, *13*(11), 759–771. http://dx.doi.org/10.1038/nrc3611
5. Wang, M., Chen, C., Gao, X., Li, J., Yue, J., Ling, F., Wang, X., & Shao, S. (2013). Distribution of Helicobacter pylori virulence markers in patients with gastroduodenal diseases in a region at high risk of gastric cancer. *Microbial Pathogenesis*, *59–60*, 13–18. https://doi.org/10.1016/j.micpath.2013.04.001
6. Backert, S., Schwarz, T., Miehlke, S., Kirsch, C., Sommer, C., Kwok, T., Gerhard, M., Goebel, U. B., Lehn, N., Koenig, W., & Meyer, T. F. (2004). Functional Analysis of the cag Pathogenicity Island in Helicobacter pylori Isolates from Patients with Gastritis, Peptic Ulcer, and Gastric Cancer. *Infection and Immunity*, *72*(2), 1043–1056. https://doi.org/10.1128/IAI.72.2.1043-1056.2004

7. Hatakeyama, M. (2019). Malignant Helicobacter pylori-Associated Diseases: Gastric Cancer and MALT Lymphoma. In S. Kamiya & S. Backert (Eds.), *Helicobacter pylori in Human Diseases: Advances in Microbiology, Infectious Diseases and Public Health Volume 11* (pp. 135–149). Springer International Publishing. https://doi.org/10.1007/5584_2019_363
8. Melenotte, C., Mezouar, S., Mège, J.-L., Gorvel, J.-P., Kroemer, G., & Raoult, D. (2020). Bacterial infection and non-Hodgkin's lymphoma. *Critical Reviews in Microbiology*, *46*(3), 270–287. https://doi.org/10.1080/1040841X.2020.1760786
9. Fanok, M. H., Sun, A., Fogli, L. K., Narendran, V., Eckstein, M., Kannan, K., Dolgalev, I., Lazaris, C., Heguy, A., Laird, M. E., Sundrud, M. S., Liu, C., Kutok, J., Lacruz, R. S., Latkowski, J.-A., Aifantis, I., Ødum, N., Hymes, K. B., Goel, S., & Koralov, S. B. (2018). Role of Dysregulated Cytokine Signaling and Bacterial Triggers in the Pathogenesis of Cutaneous T-Cell Lymphoma. *Journal of Investigative Dermatology*, *138*(5), 1116–1125. https://doi.org/10.1016/j.jid.2017.10.028
10. Hu, B., Elinav, E., Huber, S., Strowig, T., Hao, L., Hafemann, A., Jin, C., Wunderlich, C., Wunderlich, T., Eisenbarth, S. C., & Flavell, R. A. (2013). Microbiota-induced activation of epithelial IL-6 signaling links inflammasome-driven inflammation with transmissible cancer. *Proceedings of the National Academy of Sciences*, *110*(24), 9862–9867. https://doi.org/10.1073/pnas.1307575110
11. Health, C. for D. and R. (2019). Allergan Recalls Natrelle Biocell Textured Breast Implants Due to Risk of BIA-ALCL Cancer. *FDA*. https://www.fda.gov/medical-devices/medical-device-recalls/allergan-recalls-natrelle-biocell-textured-breast-implants-due-risk-bia-alcl-cancer

12. Kadin, M. E., Deva, A., Xu, H., Morgan, J., Khare, P., MacLeod, R. A. F., Van Natta, B. W., Adams, W. P., Jr., Brody, G. S., & Epstein, A. L. (2016). Biomarkers Provide Clues to Early Events in the Pathogenesis of Breast Implant-Associated Anaplastic Large Cell Lymphoma. *Aesthetic Surgery Journal*, *36*(7), 773–781. https://doi.org/10.1093/asj/sjw023

13. Hu, H., Jacombs, A., Vickery, K., Merten, S. L., Pennington, D. G., & Deva, A. K. (2015). Chronic Biofilm Infection in Breast Implants Is Associated with an Increased T-Cell Lymphocytic Infiltrate: Implications for Breast Implant–Associated Lymphoma. *Plastic and Reconstructive Surgery*, *135*(2), 319–329. https://doi.org/10.1097/PRS.0000000000000886

14. Jones, P., Mempin, M., Hu, H., Chowdhury, D., Foley, M., Cooter, R., Adams, W. P. J., Vickery, K., & Deva, A. K. (2018). The Functional Influence of Breast Implant Outer Shell Morphology on Bacterial Attachment and Growth. *Plastic and Reconstructive Surgery*, *142*(4), 837–849. https://doi.org/10.1097/PRS.0000000000004801

15. Mempin, M., Hu, H., Chowdhury, D., Deva, A., & Vickery, K. (2018). The A, B and C's of Silicone Breast Implants: Anaplastic Large Cell Lymphoma, Biofilm and Capsular Contracture. *Materials*, *11*(12), 2393. https://doi.org/10.3390/ma11122393

16. Makaremi, S., Luu, H., Boyle, J. P., Zhu, Y., Cerson, C., Bowdish, D. M. E., & Moran-Mirabal, J. M. (2019). The Topography of Silica Films Modulates Primary Macrophage Morphology and Function. *Advanced Materials Interfaces*, *6*(21), 1900677. https://doi.org/10.1002/admi.201900677

17. Wójciak-Stothard, B., Curtis, A., Monaghan, W., Macdonald, K., & Wilkinson, C. (1996). Guidance and Activation of Murine Macrophages by Nanometric Scale

Topography. *Experimental Cell Research*, *223*(2), 426–435. https://doi.org/10.1006/excr.1996.0098

18. Christo, S. N., Bachhuka, A., Diener, K. R., Mierczynska, A., Hayball, J. D., & Vasilev, K. (2016). The Role of Surface Nanotopography and Chemistry on Primary Neutrophil and Macrophage Cellular Responses. *Advanced Healthcare Materials*, *5*(8), 956–965. https://doi.org/10.1002/adhm.201500845
19. Wang, M., Chen, F., Tang, Y., Wang, J., Chen, X., Li, X., & Zhang, X. (2022). Regulation of macrophage polarization and functional status by modulating hydroxyapatite ceramic micro/nano-topography. *Materials & Design*, *213*, 110302. https://doi.org/10.1016/j.matdes.2021.110302
20. Li, K., Lv, L., Shao, D., Xie, Y., Cao, Y., & Zheng, X. (2022). Engineering Nanopatterned Structures to Orchestrate Macrophage Phenotype by Cell Shape. *Journal of Functional Biomaterials*, *13*(1), 31. https://doi.org/10.3390/jfb13010031
21. Vassey, M. J., Figueredo, G. P., Scurr, D. J., Vasilevich, A. S., Vermeulen, S., Carlier, A., Luckett, J., Beijer, N. R. M., Williams, P., Winkler, D. A., de Boer, J., Ghaemmaghami, A. M., & Alexander, M. R. (2020). Immune Modulation by Design: Using Topography to Control Human Monocyte Attachment and Macrophage Differentiation. *Advanced Science*, *7*(11), 1903392. https://doi.org/10.1002/advs.201903392
22. Chen, S., Jones, J. A., Xu, Y., Low, H.-Y., Anderson, J. M., & Leong, K. W. (2010). Characterization of topographical effects on macrophage behavior in a foreign body response model. *Biomaterials*, *31*(13), 3479–3491. https://doi.org/10.1016/j.biomaterials.2010.01.074

23. Bartneck, M., Schulte, V. A., Paul, N. E., Diez, M., Lensen, M. C., & Zwadlo-Klarwasser, G. (2010). Induction of specific macrophage subtypes by defined micro-patterned structures. *Acta Biomaterialia*, *6*(10), 3864–3872. https://doi.org/10.1016/j.actbio.2010.04.025

24. Paul, N. E., Skazik, C., Harwardt, M., Bartneck, M., Denecke, B., Klee, D., Salber, J., & Zwadlo-Klarwasser, G. (2008). Topographical control of human macrophages by a regularly microstructured polyvinylidene fluoride surface. *Biomaterials*, *29*(30), 4056–4064. https://doi.org/10.1016/j.biomaterials.2008.07.010

25. Ivanova, E. P., Hasan, J., Webb, H. K., Truong, V. K., Watson, G. S., Watson, J. A., Baulin, V. A., Pogodin, S., Wang, J. Y., Tobin, M. J., Löbbe, C., & Crawford, R. J. (2012). Natural Bactericidal Surfaces: Mechanical Rupture of Pseudomonas aeruginosa Cells by Cicada Wings. *Small*, *8*(16), 2489–2494. https://doi.org/10.1002/smll.201200528

26. Watson, G. S., Green, D. W., Schwarzkopf, L., Li, X., Cribb, B. W., Myhra, S., & Watson, J. A. (2015). A gecko skin micro/nano structure – A low adhesion, superhydrophobic, anti-wetting, self-cleaning, biocompatible, antibacterial surface. *Acta Biomaterialia*, *21*, 109–122. https://doi.org/10.1016/j.actbio.2015.03.007

27. Wang, X., Bhadra, C. M., Dang, T. H. Y., Buividas, R., Wang, J., Crawford, R. J., Ivanova, E. P., & Juodkazis, S. (2016). A bactericidal microfluidic device constructed using nano-textured black silicon. *RSC Advances*, *6*(31), 26300–26306. https://doi.org/10.1039/C6RA03864F

28. Hasan, J., Raj, S., Yadav, L., & Chatterjee, K. (2015). Engineering a nanostructured "super surface" with superhydrophobic and superkilling properties. *RSC Advances*, *5*(56), 44953–44959. https://doi.org/10.1039/C5RA05206H

29. Pogodin, S., Hasan, J., Baulin, V. A., Webb, H. K., Truong, V. K., Phong Nguyen, T. H., Boshkovikj, V., Fluke, C. J., Watson, G. S., Watson, J. A., Crawford, R. J., & Ivanova, E. P. (2013). Biophysical Model of Bacterial Cell Interactions with Nanopatterned Cicada Wing Surfaces. *Biophysical Journal*, *104*(4), 835–840. https://doi.org/10.1016/j.bpj.2012.12.046

30. Chung, K. K., Schumacher, J. F., Sampson, E. M., Burne, R. A., Antonelli, P. J., & Brennan, A. B. (2007). Impact of engineered surface microtopography on biofilm formation of Staphylococcus aureus. *Biointerphases*, *2*(2), 89–94. https://doi.org/10.1116/1.2751405

31. Hou, S., Gu, H., Smith, C., & Ren, D. (2011). Microtopographic Patterns Affect Escherichia coli Biofilm Formation on Poly(dimethylsiloxane) Surfaces. *Langmuir*, *27*(6), 2686–2691. https://doi.org/10.1021/la1046194

32. Perera-Costa, D., Bruque, J. M., González-Martín, M. L., Gómez-García, A. C., & Vadillo-Rodríguez, V. (2014). Studying the Influence of Surface Topography on Bacterial Adhesion using Spatially Organized Microtopographic Surface Patterns. *Langmuir*, *30*(16), 4633–4641. https://doi.org/10.1021/la5001057

33. Lee, S. W., Carnicelli, J., Getya, D., Gitsov, I., Phillips, K. S., & Ren, D. (2021). Biofilm Removal by Reversible Shape Recovery of the Substrate. *ACS Applied Materials & Interfaces*, *13*(15), 17174–17182. https://doi.org/10.1021/acsami.0c20697

34. Gu, H., Lee, S. W., Carnicelli, J., Zhang, T., & Ren, D. (2020). Magnetically driven active topography for long-term biofilm control. *Nature Communications*, *11*(1), 2211. https://doi.org/10.1038/s41467-020-16055-5

35. Lee, S. W. (2020). *Effects of Surface Topography on Bacterial Biofilm Formation* (Order No. 28088082). Available from Dissertations & Theses @ Syracuse University; ProQuest Dissertations & Theses Global. (2446082773). https://libezproxy.syr.edu/login?url=https://www.proquest.com/dissertations-theses/effects-surface-topography-on-bacterial-biofilm/docview/2446082773/se-2?accountid=14214

36. Möller, J., Luehmann, T., Hall, H., & Vogel, V. (2012). The Race to the Pole: How High-Aspect Ratio Shape and Heterogeneous Environments Limit Phagocytosis of Filamentous Escherichia coli Bacteria by Macrophages. *Nano Letters*, *12*(6), 2901–2905. https://doi.org/10.1021/nl3004896

Vita

Joseph Carnicelli

Education:

2017, Bachelors of Science, Biomedical Engineering

Binghamton University

2018, Masters of Engineering, Biomedical Engineering

Cornell University

Publications:

Lee, S. W., Carnicelli, J., Getya, D., Gitsov, I., Phillips, K. S., & Ren, D. (2021). Biofilm Removal by Reversible Shape Recovery of the Substrate. *ACS Applied Materials & Interfaces*, *13*(15), 17174–17182. https://doi.org/10.1021/acsami.0c20697

Gu, H., Lee, S. W., Carnicelli, J., Zhang, T., & Ren, D. (2020). Magnetically driven active topography for long-term biofilm control. *Nature Communications*, *11*(1), 2211. https://doi.org/10.1038/s41467-020-16055-5

Gu, H., Lee, S. W., Carnicelli, J., Jiang, Z., & Ren, D. (2019). Antibiotic Susceptibility of Escherichia coli Cells during Early-Stage Biofilm Formation. *Journal of Bacteriology*, *201*(18). https://doi.org/10.1128/JB.00034-19